Exclusive Studies of Short Range Correlations in Nuclei using CLAS12
Proposal to Jefferson Lab PAC 46

A. Ashkenazy, R. Cruz Torres, S. Gilad, O. Hen (contact person),
G. Laskaris, A. Papadopoulou, M. Patsyuk, A. Schmidt (co-spokesperson),
B. Schmookler, and E.P. Segarra
Massachusetts Institute of Technology, Cambridge, MA

F. Hauenstein, M. Hattawy, C. Hyde, M. Khachatryan,
S. Kuhn, and L.B. Weinstein (co-spokesperson)
Old Dominion University, Norfolk VA

E.O. Cohen, M. Duer, and E. Piasetzky (co-spokesperson)
Tel-Aviv University, Tel Aviv, Israel

D. Higinbotham, S. Stepanyan (co-spokesperson),
H. Szumila-Vance (co-spokesperson), and S.A. Wood
Thomas Jefferson National Accelerator Facility, Newport News, VA

Christopher Marshall
Lawrence Berkeley National Laboratory, Berkeley, CA

K. Mahn, J. Morrison, L. Pickering
Michigan State University, East Lansing, MI

A. Beck, I. Korover, and S. Mey-Tal Beck
Nuclear Research Negev, Israel

A. El Alaoui, H. Hakobian, T. Mineeva, J. Miller, and W. Brooks
Universidad Tecnica Federico Santa Maria (UTFSM), Valparaiso, Chile

M. Betancourt
Fermi National Accelerator Laboratory, Batavia, IL

T. Katori
Queen Mary University, London, Great Britain

I. Balossino, L. Barion, G. Ciullo, M. Contalbrigo,
P. Lenisa, A. Movsisyan, and L.L. Pappalardo
INFN Ferrara and University of Ferrara, Ferrara, Italy

D. Watts and L. Zana
Edinburgh University, Edinburgh, Scotland

D. Ireland and D. Sokhan
Glasgow University, Glasgow, Scotland

N. Kalantarians
Virginia Union University, Richmond, VA

S. Li
University of New Hampshire, Durham, NH

and the CLAS12 Collaboration
(Dated: June 4, 2018)

Abstract

Short-ranged correlated (SRC) nucleon-nucleon (NN) pairs account for about 20% of all nucleons in medium to heavy nuclei and about 75% of the nuclear kinetic energy. In addition, there is strong evidence linking these pairs to nucleon structure modification in nuclei (the EMC effect). A significant amount of our knowledge of SRC pairs comes from hard two nucleon knockout measurements, conducted using electron (i.e. $(e, e'pp)$ and $(e, e'pn)$) and proton probes (i.e. $(p, 2pn)$). These studies show that almost all high-momentum nucleons belong to SRC pairs, that these pairs are predominantly pn pairs in all measured nuclei, that pair center-of-mass momentum distributions is small, and that increasing the neutron fraction increases the probability that a proton in the nucleus belongs to a correlated pair.

These discoveries were extracted from remarkably small data samples, containing only a few dozen to a few hundred $(e, e'pN)$ events on each measured nucleus. There are many open questions in SRC studies that can only be addressed via high-statistics studies of selected nuclei. These include the existance and properties of Three-Nucleon SRCs, constraining the NN interaction and ab-initio calculations of the nuclear wave function at short distances, understanding factorized effective theories and effective SRC formation mechanisms, studies of three-nucleon correlations, and exploring the detailed connection of SRCs and the EMC effect. This proposal sets to address these and other outstanding issues by preforming new measurements of SRCs using exclusive reactions at Hall B with the CLAS12 spectrometer. We expect an increase in statistics of x10 to x40 as compared to existing 6 GeV data. In addition, the large count rates in conjunction with the use of different beam energies and the wide acceptance of CLAS12 provides an increased kinematical coverage, allowing for a 3N-SRC search in exclusive reactions, detailed studies of Q^2 and kinematical dependencies, as well as the mass-number (A) and nuclear asymmetry (N/Z) dependencies of SRCs.

We request 38 PAC days at Hall B using CLAS12 at with 4.4 GeV and 6.6 GeV beam energies on ^{2}H, ^{4}He, C, Si, ^{40,48}Ca , Sn and Pb.

I. INTRODUCTION

Short-range correlations, pairs of nucleons with high relative and low center-of-mass (c.m.) momentum, are an integral part of the nuclear medium. Nucleons at short distance experience a strong short-ranged interaction, generating a high-momentum tail in the nuclear wave function that extends significantly above the Fermi-momentum. The creation of such a high-momentum tail, due to the strong short-ranged interaction, is a universal feature of atomic nuclei and nuclear matter. Recent works have shown that short-range correlations (SRCs) in atomic nuclei account for approximately 20% of the nucleons in the nucleus and are predominantly neutron-proton pairs [1–12]. As nucleons are composite objects, their internal structure may well be modified when the distance between them is smaller than their radii, causing substantial overlap between their quark distributions. SRC research therefore lies on the border between nuclear and bound nucleon structure.

The short-range structure of nuclei is a vibrant field of research. The most recent result of these studies was just accepted for publication in Nature, with previous results published in Science, PRL, Physics Letters, PRC, PRD and more. SRC studies were also shown to have implications for many other topics, including quark distributions in nuclei (the EMC effect) and the free neutron structure [1, 13–17], nuclear symmetry energy and neutron star structure [5, 18–20], nuclear charge radii and the neutron skin of neutron-rich nuclei [21], energy sharing and correlations in ultra-cold two-component Fermi-gases [6, 22, 23], the analysis of low-energy (≈ 50 MeV/A) heavy-ion collisions [18, 19], neutrino-nucleus interactions and the analysis of next-generation neutrino oscillation experiments [24, 25], pairing mechanisms and scale separation in nuclei [26, 27], and nuclear correlation functions and double beta decay [27, 28].

These results, and others, stimulated a significant theoretical effort that vastly improved our ability to model and calculate SRCs, and estimate their impact on various phenomena. As theory has advanced, existing data have become insufficient for guiding and constraining it. Specifically, current SRC data sets from the JLab 6 GeV program contain, at most, a few hundreds of exclusive events, on only a handful of nuclei. We propose here to make a significant and needed improvement by studying SRCs with unprecedented accuracy using exclusive and semi-inclusive hard scattering reactions at Hall B, using CLAS12 in its standard configuration, at beam energies of 4.4 GeV and 6.6 GeV. The new measurement will improve on existing data by one to two orders of magnitude in statistics, while adding new nuclei of interest. The proposed measurement may also run as a run group with PAC45 conditionally approved 'Electrons for Neutrinos' proposal.

The experiment proposes to measure one (i.e. $(e, e'N)$), two (i.e. $(e, e'NN)$), and three (i.e. $(e, e'ppN)$) nucleon knockout reactions in kinematics dominated by the hard breakup of two- and three-nucleon SRCs in selected of target nuclei. The data will be used to study:

1. NN interaction and the nuclear wave function at short distances,
2. SRC pair formation mechanisms,
3. Nuclear asymmetry dependence of SRCs,
4. Three-Nucleon SRCs,
5. Reaction mechanisms (QE nucleon knockout),
6. EMC Effect and its relation to SRCs.

The proposal layout is as follows: chapter II reviews recent results from experimental and theoretical studies of SRCs, chapter III details the physics goals of the current proposal, chapter IV describes the main features of nucleon knockout reactions and their applicability for SRC studies, and chapter V details the proposed experimental setup, kinematical coverage and expected event rates.

II. OVERVIEW OF RECENT RESULTS

The study of short-range correlations is a broad subject, covering a large body of experimental and theoretical work, as well as phenomenological studies of the implications of SRCs for other phenomena in nuclear, particle and astro-physics. A full discussion of SRC physics is available in a recent RMP review [1] and a recent theory-oriented review [2].

The results presented below are based on measurements of high-energy electron scattering in large-momentum transfer kinematics (i.e. hard scattering). These measurements' resolving power is determined by their momentum transfer, and their interpretation relies on the theoretical modeling of the interaction. The latter should account for all possible reaction mechanisms that lead to the same measured final state. High-momentum transfer measurements

can therefore be viewed in several ways. The discussion below views the electron interaction in terms of Quasi-Elastic (QE) scattering off single nucleons, which is the simplest reaction picture that is consistent with both the measured observables [1, 2, 4, 5] and various reaction and ground-state ab-initio calculations [3, 29]. Nuclei can also be described in a picture in which the probe interacts with a simpler ground state, though with more complex short-distance multi-nucleon operators. In this case, the complexity of the wave function is converted to the complexity of the operators through a unitary transformation [30]. In this picture, the proposed measurements can be used to constrain the resulting short-distance physics. While discussing the proposed measurements in the first picture, the two pictures are physically equivalent.

A. Hard-knockout reaction measurements and short-distance Tensor interactions

1. *NN Interaction and nuclear wave function (experiment)*

Over the last decade, we have learned a remarkable amount about SRCs with remarkably few events, obtained from measurements of exclusive hard knockout reactions, $A(e,e'N)$ and $A(e,e'pN)$ [6–8, 31, 32] (here N stands for neutron or proton), from selected nuclei (^{4}He, C, Al, Fe and Pb). The electrons in these reactions interacted with protons or neutrons in the target nucleus via a high-momentum transfer reaction ($Q^2 > 1.7 - 2$ GeV^2), leading to the knockout of a high-momentum nucleon and, in certain events, the simultaneous emission of a correlated recoil nucleon.

The first such exclusive measurements of SRC pair breakup reactions were performed using hadronic (proton) [9, 33] and electronic [8, 34] probes on C (Fig. 1, bottom left panel). The main results of these studies are:

- Within statistical uncertainties of about 20%, all knocked-out protons with missing-momentum (reconstructed initial momentum in the absence of re-interactions) in the range of 300–600 MeV/c have an associated recoil nucleon with a momentum that balances the missing momentum.
- These recoil nucleons are almost entirely neutrons. Neutron-proton (np) pairs are nearly 20 times more prevalent than proton-proton (pp) pairs, and by inference, neutron-neutron (nn) pairs.
- The relative momenta of the SRC pairs, as reconstructed from the missing and recoil-nucleon momenta, are higher than k_F, while the c.m. momenta are lower (k_F is the nuclear Fermi momentum, typically about 250 MeV/c for medium to heavy nuclei). The latter was observed to be consistent with a Gaussian distribution with characteristic width of about 140 MeV/c.

One common interpretation of these results is that the nucleon momentum distribution above k_F is dominated by np-SRC pairs [1, 2, 4, 5]. The predominance of np-SRC pairs over pp-SRC pairs suggests that the tensor part of the NN interaction is dominant at the probed distances [2, 36–38]. The tensor interaction is proportional to the total spin of the pair, S. As such, $S = 1$ states (spin-symmetric states with both spins pointing in the same direction) are preferred over the $S = 0$ (the equivalent spin-asymmetric) states. As SRC pairs are primarily in a relative S- or D-wave (i.e. even L, symmetric configuration), their isospin must be zero (asymmetric) due to the Pauli principle. Therefore, the tensor force favors np-SRCs, which have an asymmetric isospin component, suppressing contributions from pp-SRC (and nn-SRC) pairs.

One should note that the tensor interaction is a longer-ranged interaction, though it is much smaller than the dominant scalar part of the NN interaction. Studies of the deuteron show that its second order effect, viewed as a two-pion exchange term, becomes comparatively more important at shorter range, where the scalar force approaches zero [1, 22]. This observation is also consistent with calculations of heavier nuclei [2, 36–38].

At even higher missing momenta, and thus smaller pair separation, the essentially unexplored repulsive scalar interaction should become dominant. We measured the ^{4}He$(e,e'p)$ and ^{4}He$(e,e'pN)$ reactions at an $(e,e'p)$ missing momenta range of 400 to 830 MeV/c [7] to study the expected transition from the tensor-dominated regime to the short-range repulsive (and presumably scalar) dominated regime. The latter should be manifested by an increase in the fraction of pp-SRC pairs. While statistically limited, the experimental results shown in Fig. 1 (top left panel) indicate an increase of the pp/np SRC ratio with missing momentum, presumably from the tensor region towards the scalar-dominated region.

More recently, we extended these studies from ^{4}He and C to include Al, Fe and Pb, as part of the JLab CLAS6 data-mining initiative. These studies were published in Science and Physics Letters [6, 31], with the most recent result just accepted for publication in Nature. The first study extracted the ratio of np to pp SRC pairs in these nuclei by measuring $A(e,e'p)$ and $A(e,e'pp)$ and assuming that all high-p_{miss} protons belonged to SRC pairs. Therefore any $(e,e'p)$ event not accompanied by the emission of a recoil proton was associated with scattering from an np-SRC pair.

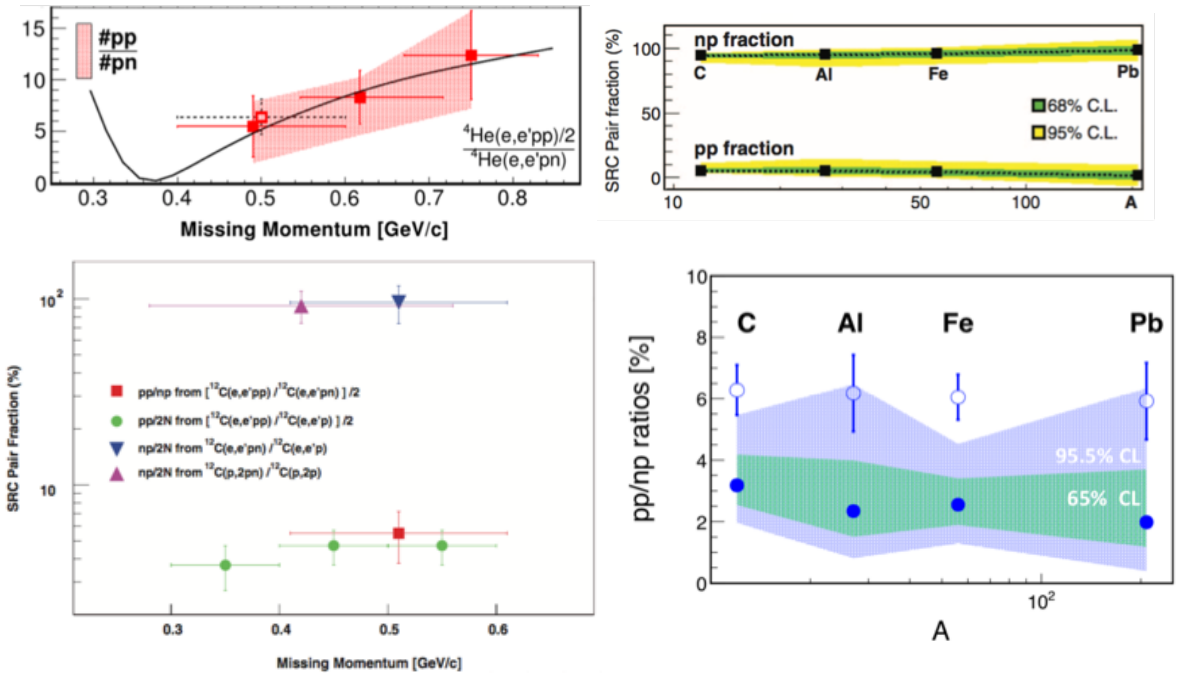

FIG. 1: Recent results on np-SRC dominance in nuclei from ^{4}He to Pb from various $A(e,e'p)$ and $A(e,e'pN)$ measurements. Bottom left: fraction of knocked-out protons with a correlated neutron (triangles) and proton partner (green circles), and the ratio of np- to pp-SRC pairs (red square) in C, extracted from $(p,2pn)$ [9, 33] and $(e,e'pN)$ [6–9, 33, 34] measurements; Top Left: missing-momentum dependence of the ratio of pn pairs to pp pairs in ^{4}He from $(e,e'pN)$ measurements [7]; Top right: fraction of knocked-out protons with a proton partner (pp pair) and, by inference, with a neutron partner (np pair) as a function of A from $(e,e'p)$ and $(e,e'pp)$ measurements [6]; Bottom right: the ratio of pp to pn SRC pairs for different nuclei from recent $(e,e'Np)$ measurements [35], before (points) and after (bands) correcting the measured cross-section ratios for reaction mechanism effects. The inner and outer bands represent the 68% and 95% confidence limits of the extracted ratios, respectively.

This, combined with previous measurements, allowed an extraction of the relative fraction of np- and pp-SRC pairs in Al, Fe and Pb (see Fig. 1, top right panel) [6].

As the extraction of Ref. [6] relied on the assumption that all high-p_{miss} protons belonged to SRC pairs, we recently complemented it by an extraction of the ratio of np to pp SRC pairs in these nuclei from a direct measurement of the $A(e,e'pp)$ and $A(e,e'np)$ reactions. The ratio of these reactions showed a similarly small ratio of pp to np SRC pairs that is consistent with the former analysis of $A(e,e'p)$ and $A(e,e'pp)$ reactions (Fig. 1, bottom right panel). The consistency of the results obtained from the two analyses supports the assumption made in the latter [35].

The extracted ratio therefore indicates that the observed predominance of np-SRCs in C persists also in the heavier nuclei. This observation was in tension with certain theoretical expectations that heavier nuclei would have a larger fraction of pp-SRC pairs due to cross-shell pairing that would allow for tensor-induced pp-SRCs.

For completeness of the discussion we note that all analyses described above include corrections for reaction mechanisms, detailed later in this section.

Further insight into the NN interaction at short distances can be obtained by examining the missing-momentum dependence of the $A(e,e'pp)/A(e,e'p)$ cross-section ratio in C, Al, Fe, and Pb. After corrections for reaction mechanisms, namely FSI and SCX (see discussion below), this ratio is sensitive to the fraction of pp-SRC pairs from all high-momentum protons. Assuming that at the measured kinematics the full $A(e,e'p)$ cross-section is exhausted by the hard breakup of SRC pairs, this ratio is also a measure of the variation in the np to pp SRC pairs ratio. Fig. 2 (left) shows a preliminary extraction of the fraction of protons in pp-SRC pairs to all high-momentum nucleons as a function of the proton momentum in the different measured nuclei. As can be seen, the extracted ratio is consistent within uncertainties from C to Pb and shows an increase from the 'tensor dominated' region at 400 - 600 MeV/c to what could be interpreted as a scalar region at 700 - 900 MeV/c.

Fig. 2 (right) shows the weighted average data from all nuclei compared with an ab-initio many-body calculation of the ratio of nuclear ground state two- to one-body momentum densities in C. The theoretical prediction is obtained from the Variational Monte-Carlo (VMC) calculations of C [39], analyzed using the 'Generalized contact formalism' [26]. As can be seen, the calculation agrees with the data in the tensor-dominated region of 400–600 MeV/c but

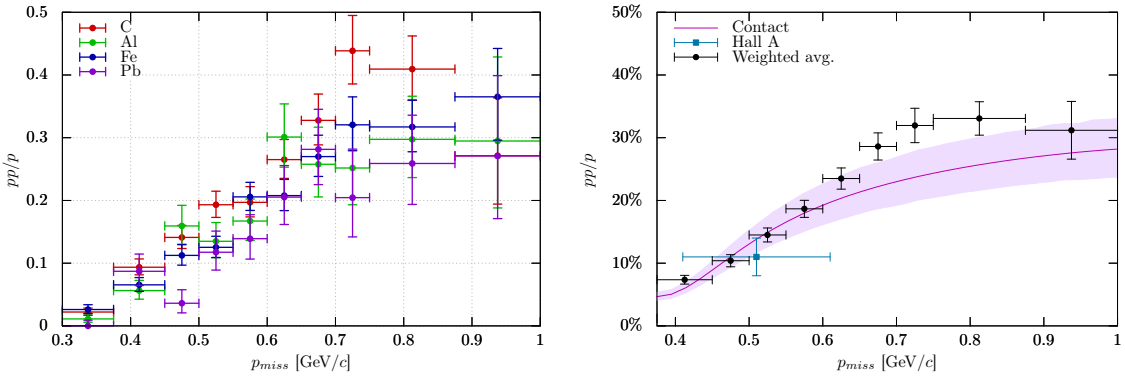

FIG. 2: (preliminary) Extracted $A(e,e'pp)/A(e,e'p)$ cross-section ratio as a function of $(e,e'p)$ missing-momentum. Left: The cross-section ratio for different nuclei are consistent within uncertainties. Right: The average for C, Al, Fe and Pb where the band shows the prediction of the ab-initio calculation of [39] using VMC technique and AV18+UIX NN and 3N interactions. The calculation is analyzed using the contact formalism [26] and corrected for reaction mechanism effects using the formalism of [40]. The calculation has no free parameters and is not normalized to the data.

starts deviating for higher missing momenta where the reaction is expected to be sensitive to the largely unexplored repulsive core of the NN interaction.

As momentum densities are not observables, the interpretation of the data in terms of such ground state densities is not trivial. Indeed, it relies on the fact that the discussed nucleon knockout measurements are carried out in kinematics where, according to calculations, reaction mechanisms other than the hard breakup of SRC pairs are suppressed and any residual effects are significantly reduced when considering cross-section ratios as opposed to absolute cross-sections [1, 4, 40–42]. At the high Q^2 of the measured nucleon knockout reactions, the cross-sections approximately factorize and calculations of Final State Interactions (FSI) and Single-Charge Exchange (SCX) of the outgoing nucleons are done using an Eikonal approximation in a Glauber framework (see [2, 43–45] and references therein). These effects are significant and must be corrected for before any comparison with ground-state calculations can be made. This is especially true when considering reactions on medium to heavy nuclei. An example for the impact of SCX is shown in Fig. 1 (bottom right panel), where the hollow points show the pp to np SRC ratios as directly extracted from the measured $(e,e'Np)$ cross-section ratios, while the bands include SCX corrections based on the formalism of [41]. As can be seen, these corrections are non-negligible and contribute to the systematic and interpretation uncertainty of the measurement. Therefore, testing and constraining these calculations is an integral part of the experimental program. An example for such tests is shown in Fig. 3, where recent extraction of cross-section ratios for $A(e,e'p)$, $A(e,e'n)$ and $A(e,e'pp)$ reactions are shown to agree well with the predictions of the above-mentioned reaction calculations [31, 41, 46, 47].

Last, it should be noted that all of these fascinating results were obtained with remarkably low statistics. As a result, while providing significant insight, they do not allow for stringent tests of modern many-body calculations. Furthermore, their kinematical reach is limited and the data does not allow for a significant test of kinematical dependencies such as Q^2 independence etc. This proposal sets to remediate this situation by providing a significant increase in statistics and a systematic study of nuclei of interest.

2. NN Interaction and nuclear wave function (theory)

From a theoretical standpoint, the dominance of np-SRC pairs over pp-SRC pairs in nuclei has been primarily studied using state-of-the-art ab-initio many-body calculations of pair momentum distribution functions for different nuclei [2, 36–38, 48, 49]. These calculations show the dominance of np pairs at relative pair momenta greater than 300 MeV/c (Fig. 4, top left panel). By considering different variations of the NN interaction, for example with and without a significant tensor force, the unique role of the latter in the relevant momentum range can be identified [36].

Recently, a 'generalized contact formalism' approach was developed to explore the underlying dynamics of SRC pairs in nuclei [26]. In this approach, the short-distance many-body wave function factorizes into a universal two-body function that depends only on the pair relative momentum (q), times a mean-field like many-body function that depends on the pair c.m. momentum (Q), instead of the states of the individual nucleons of the pair. This factorization stems from the separation between short-distance scales, responsible for the pair relative momentum,

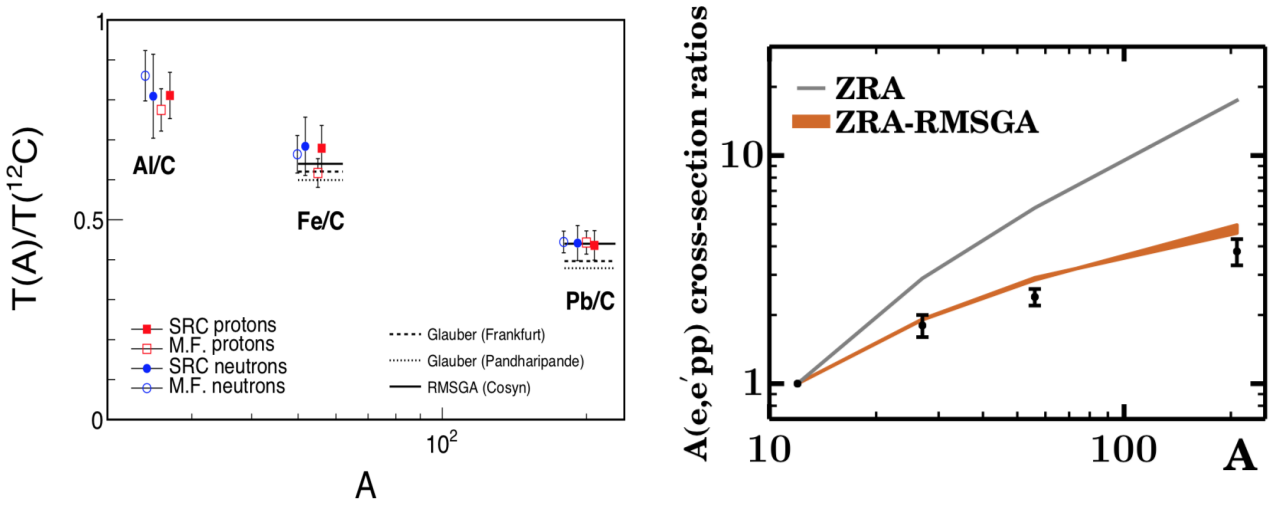

FIG. 3: Recent measurement of transparency ratios for nuclei relative to C, as obtained from measurements of A(e,e'p) and A(e,e'n) reactions in kinematics corresponding to knockout of mean-field and SRC nucleons (left), and A(e,e'pp) reaction in kinematics corresponding to hard breakup of *pp*-SRC pairs (right) [40]. The measurements show good agreement with several theory predictions that are based on a Glauber approximation [41, 46, 47].

and longer-distance scales associated with the nuclear many-body dynamics affecting the total number of pairs and their c.m. momentum distribution. This new formalism was successfully bench-marked against state-of-the-art VMC and Cluster-VMC calculations of nuclei from ^{4}He to ^{40}Ca in both momentum and coordinate space [26].

Fig. 4 (top right panel) shows good agreement between the generalized contact-formalism predictions (black solid and dashed lines), and the measured ^{4}He pp/np SRC pairs ratio [26]. Also shown are two-body densities obtained from many-body Variational Monte Carlo (VMC) calculations using the AV-18 and UIX two and three body interactions (colored solid lines). The calculated densities are shown as a function of the pair relative momentum, integrated over the pair c.m. momentum from zero to k_{max}. The latter varies from zero to infinity. As can be seen, as long as the maximum c.m. momentum is smaller than k_F, the calculated ratio describes the experimental data well.

Recent VMC calculations of one- and two-body densities using the N2LO interaction show that while the momentum densities are scale and scheme dependent, ratios of *np* to *pp* SRC pair abundances are scale and scheme independent and overall agree with $A(e,e'pN)$ data (Fig. 4, bottom right panel) [29]. While the accuracy of both the data and the calculations is statistically limited, the calculation should improve significantly in the near future. This proposal seeks to provide similar improvement to the data.

The factorized approach of the generalized contact formalism was recently extended to model the high-momentum part (i.e. continuum states) of the nuclear spectral function. Fig. 4 (bottom left panel) shows the calculated ratio of *pp* to *np* SRC pairs in ^{4}He as a function of both missing energy and momentum as obtained from the spectral function of the contact formalism. The calculation is compared to the measured ^{4}He$(e,e'pN)$ data that, for the first time, show good agreement in the missing energy dependence as well. However, the statistical uncertainties of the data are significant, and better data will allow more stringent tests of the details of the calculation. One should note that similar calculations using the N3LO potential also show good agreement with the data, supporting the observation of reduction of the scale and scheme dependence of the interaction in the formation of ratios.

It should be stressed that moving from momentum densities to effective spectral functions has significant implications to various aspects of the JLab program, including DIS and nuclear DVCS processes off nuclei that require spectral functions or light-cone densities that are derived from them [1, 50]. From a nuclear structure point of view, the spectral function contains additional information that is very hard to access in an integrated momentum density, such as the *pp* wave-function deep in the high-momentum tail region.

The observed agreement of the data with the factorized contact calculations in both momentum density and spectral function frameworks will thus allow us to relate the SRC isospin to the underlying properties of the NN interaction at short distances. Both the data and the calculations show clearly the transition from a small pp/np ratio, a fingerprint of the tensor interaction, to the expected pp/np ratio for scalar interaction. However, more precise data are needed to improve our insight and challenge the calculations.

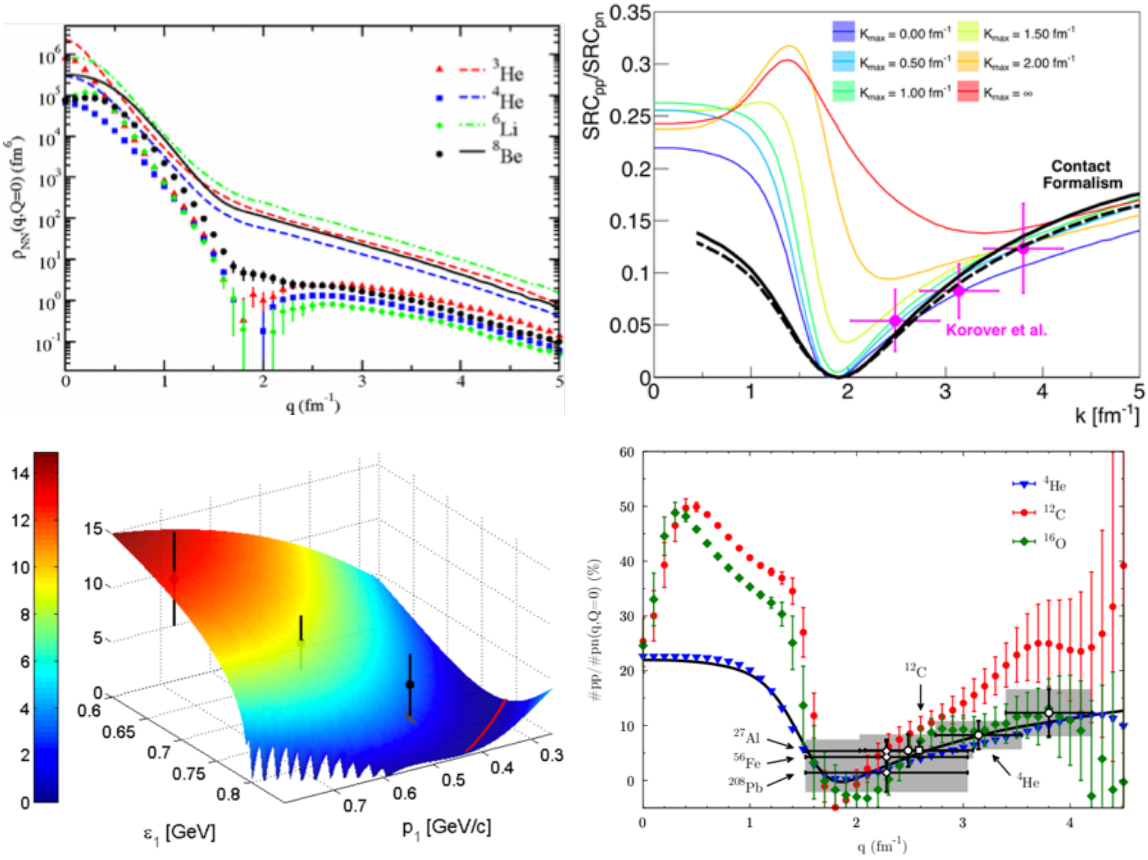

FIG. 4: Top Left: calculated *np* (lines) and *pp* (points) stationary pair momentum density in light nuclei [36]. Top Right: measured and calculated ^{4}He *pp*/*np* pair density ratios as a function of the pair relative momentum for different regions of integration over the pair c.m. momentum k [26]. Bottom Right: the ratio of *pp* to *np*-pairs with zero c.m. momentum Q as a function of relative momentum q for N2LO two body momentum densities and for data. Bottom Left: spectral function ratio compared with ^{4}He$(e, e'pN)$ data.

3. *Effective SRC pair formation mechanisms*

The properties of SRC pairs (e.g., abundances and c.m. momentum distributions) across different nuclei can provide valuable insight into the underlying effective pair formation mechanisms and the relation between the SRC-induced, high-momentum continuum states and the undelying low-energy shell structure of nuclei. Specifically, one can model the single-nucleon momentum distributions at high-momenta by shifting the complexity induced by SRCs from the wave functions to correlation operators acting on mean-field nucleon pairs. For example, one such model predicts that the SRC-related high-momentum tail of the single-nucleon momentum distribution is dominated by correlation operators acting on mean-field pairs with zero relative radial and angular momentum quantum numbers ($n = 0$, $l = 0$) [40, 44].

To test this model and others, it is instructive to examine how the properties SRCs vary across a wide range of different nuclei. Fig. 5 (left panel) shows a calculation of the number of SRC pairs in different nuclei relative to C, assuming different models for the mean-field nucleons that can correlate to form SRC pairs. The calculations are compared to $A(e, e'pp)$ and $A(e, e'p)$ data on C, Al, Fe and Pb that allowed direct extraction of the number of *pp*-SRC pairs and indirect extraction of the number of *np*-SRC pairs. A follow-up analysis recently extracted $A(e, e'Np)$ cross-section ratios, directly measuring both *pp* and *np*-SRC pairs (Fig. 5, right panel). The results show a linear increase in the number of SRC pairs - both *pp* and *pn* SRC pairs as a function of nuclear size, in overall agreement with both a Zero-Range Approximation model (ZRA) and the $n = 0$, $l = 0$ model. However, better data is needed to make more quantitative statements about SRC pair formation processes.

A complementary view of the quantum numbers of mean-field pairs that fluctuate to form SRC pairs can be obtained by examining the c.m. momentum of SRC pairs, which is induced by the mean-field like interaction of the pair with the residual A-2 nuclear system. Fig. 6 shows new results from the extraction of the c.m. momentum distribution of *pp*-SRC pairs from a recent analysis of $A(e, e'pp)$ data recently submitted for publication [51]. The extracted

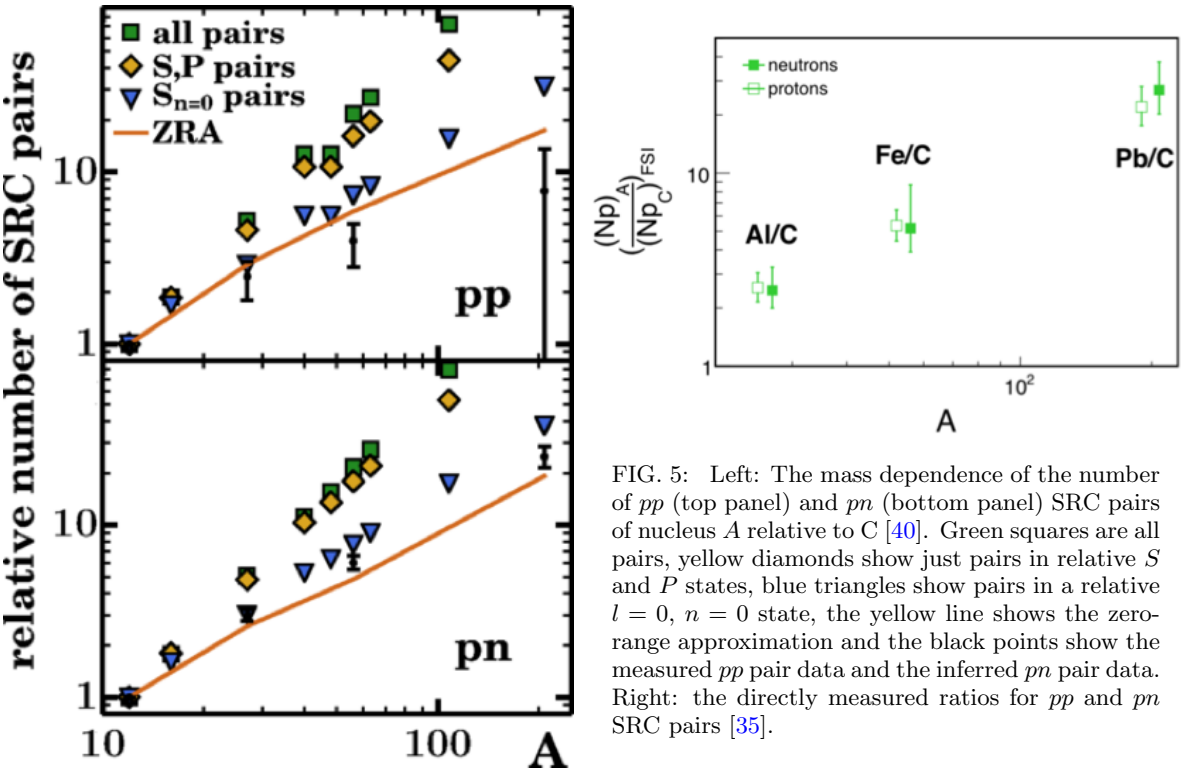

FIG. 5: Left: The mass dependence of the number of pp (top panel) and pn (bottom panel) SRC pairs of nucleus A relative to C [40]. Green squares are all pairs, yellow diamonds show just pairs in relative S and P states, blue triangles show pairs in a relative $l = 0$, $n = 0$ state, the yellow line shows the zero-range approximation and the black points show the measured pp pair data and the inferred pn pair data. Right: the directly measured ratios for pp and pn SRC pairs [35].

c.m. momentum distribution for C, Al, Fe and Pb is consistent with a Gaussian distribution in each direction. The extracted Gaussian width varies between 140 and 170 MeV/c, and is constant within uncertainties. It is also consistent with both a simple Fermi-gas model expectation of 150 MeV/c (where the NN pair is formed from two randomly chosen nucleons, assuming $k_F = 250$ MeV/c) and more realistic mean-field calculations [44, 52]. The success of mean-field calculations in describing the c.m. momentum distribution of SRC pairs gives important support to the factorized approach of the generalized contact formalism and its applicability in relating measured quantities with ab-initio ground state calculations. In addition, the data seems to be higher than the mean-field predictions that assume all NN pairs can form SRC pairs, but lower than the most restrictive $^1S_0$ calculation. This might indicate some selectivity in the SRC pairs formation process. However, the accuracy of the current data is insufficient to make a definitive claim between the models.

We note that momentum densities are not observables and it is therefore impossible to 'measure' the c.m. or relative momentum density of SRC pairs. In the study presented here, only the width of the c.m. momentum density distribution was extracted. Fortunately, this width is robust to many reaction mechanism effects, e.g., SCX and FSI, that lead to flux reduction, i.e., transparency. This claim is supported by both reaction calculations that show the c.m. width is largely insensitive to reaction effects [41, 44] and by the lack of significant broadening of the distribution from C to Pb in the data itself, which could be expected if there were significant soft rescattering of the SRC nucleons by the $A-2$ system. See Ref. [44, 51] and references therein for additional details and an extended discussion.

Last, it should be noted that a recent calculation [21] showed that SRC pairs could have a significant impact on ab-initio calculations of the proton and neutron radii in neutron-rich nuclei, thereby possibly impacting the extraction of the neutron skin of nuclei, and consequently the nuclear symmetry energy. Constraining the exact modeling of SRC pairs in terms of correlation operators acting on mean-field NN pairs will have direct impact on such calculations.

B. Nuclear asymmetry dependence of short-ranged correlations

The predominance of np-SRC pairs leads to interesting phenomena in asymmetric nuclei. Without SRC pairs, neutrons in neutron-rich nuclei should have higher Fermi momentum and thus a higher average momentum and kinetic energy than the minority protons. However, as SRCs produce high-momentum tail comprised predominantly of np-pairs, they should lead to an equal number of protons and neutrons above k_F. Therefore, the excess neutrons in a neutron-rich nucleus should either increase the fraction of correlated protons or occupy low-momentum states. In either case, the fraction of high-momentum protons should be larger than that of neutrons [6, 23].

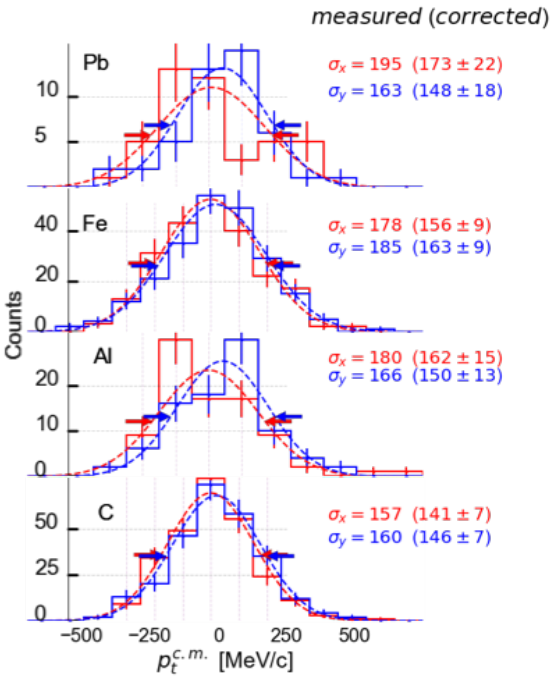

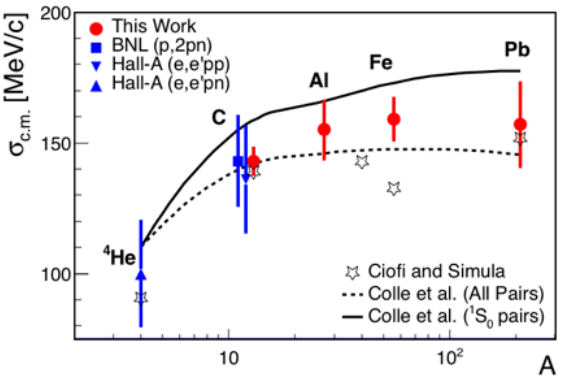

FIG. 6: Left: the extracted pp-SRC pairs c.m. momentum distribution as obtained from $A(e,e'pp)$ measurements. Right: the extracted width of the pp-SRC c.m. momentum distribution, assuming normal distribution and after finite detector acceptance corrections. The lines and stars represent various theoretical predictions [44, 52]. See Ref. [51] for details.

We recently reported on a simultaneous measurement of hard QE electron scattering off protons and neutrons (i.e. $A(e,e'p)$ and $A(e,e'n)$ reactions) in A = C, Al, Fe, and Pb nuclei [32]. The simultaneous measurement of both proton and neutron knockout allowed a direct comparison of their properties with only minimal assumptions.

The measurement was made in two kinematical settings, corresponding to electron-scattering primarily off nucleons either from SRC pairs (missing momentum $> k_F$) or from the nucleons in the mean-field region (missing momentum $< k_F$). Using these event samples, the reduced cross-section ratios: $[A(e,e'n)/\sigma_{en}]/[A(e,e'p)/\sigma_{ep}]$ (i.e. measured cross-sections divided by the known elementary electron-proton σ_{ep} and electron-neutron σ_{en} cross-sections) were extracted for each kinematical setting. The results shown in Fig. 7 (left) indicate that the n/p mean-field reduced cross-section ratios grow approximately as N/Z for all nuclei, as expected from simple nucleon counting. However, the SRC ratios in all nuclei are consistent with unity, as expected from np-dominance.

To quantify the pairing mechanism leading to constant n/p ratios for SRC nucleons, we also extracted the relative fraction of high-missing-momentum to low-missing-momentum events in neutron-rich nuclei relative to ^{12}C, see Fig. **??** (right). This extraction was done separately for protons and neutrons and shows that the neutron SRC probabilities are independent of the nuclear neutron excess (i.e., they saturate) while the corresponding proton fractions grow linearly with N/Z. This observation indicates that the excess outer neutrons in a neutron-rich nucleus form SRC pairs with protons from the inner core.

As a complement to that study, in April 2018, JLab experiment E12-14-011 [53] measured electron-induced proton knockout, $(e,e'p)$, from ^{3}H and ^{3}He at large Q^2 (> 1.8 GeV/c^2), x_B >1 anti-parallel kinematics, shown to minimize contributions from FSI and other competing effects [4, 40, 42, 43, 54]. This will permit an extraction of the ratio of the proton momentum densities in ^{3}He and ^{3}H as a function of missing momentum with minimal dependence on theoretical corrections.

C. The EMC Effect and Short-Ranged Correlations

The relative abundance of SRC pairs in nuclei can be extracted from measurements of inclusive (e,e') cross-section ratios for different nuclei at $Q^2 > 1.4$ GeV^2 and $x_B > 1$ [1, 2, 4, 5, 10–12]. For a fixed value of Q^2, when plotted as a function of x_B, these cross-section ratios scale starting approximately at $x_B \geq 1.5$.

The height of the scaling plateau can be used to extract the relative number of high-momentum nucleons (i.e., SRC pairs) in the measured nuclei. We refer to these as the SRC scaling coefficients.

The extracted SRC scaling coefficients linearly correlate with the EMC effect in nuclei from ^{3}He to ^{197}Au [1, 14–16]. The latter is the slope of the deviation from unity of the isoscalar DIS cross-section ratio for nuclei relative to deuterium for $0.3 \leq x_B \leq 0.7$. The EMC effect is commonly interpreted as evidence for modification of the partonic structure function of bound nucleons.

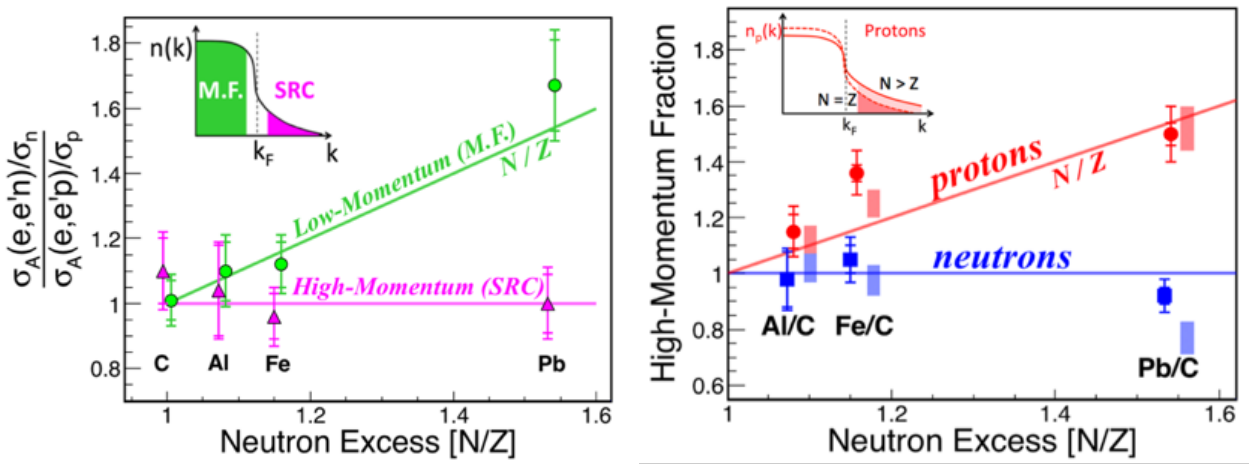

FIG. 7: Results from recent proton and neutron knockout measurements [32]. Left: extracted ratio of neutron to proton knockout from above and below the nuclear Fermi momentum, k_F. Right: Extracted fraction of high-momentum ($k > k_F$) protons and neutrons in neutron-rich nuclei relative to Carbon.

The modification of the internal structure of bound nucleons due to the influence of the nuclear medium is of vast interest for QCD research and can provide new insight into the fundamental mechanism of confinement. As of today, the EMC effect is the only concrete, well-established and well-studied experimental evidence we have for such modification. However, even though it was first observed over 35 years ago, the origin of the EMC effect is still an open puzzle at the interface of nuclear and particle physics.

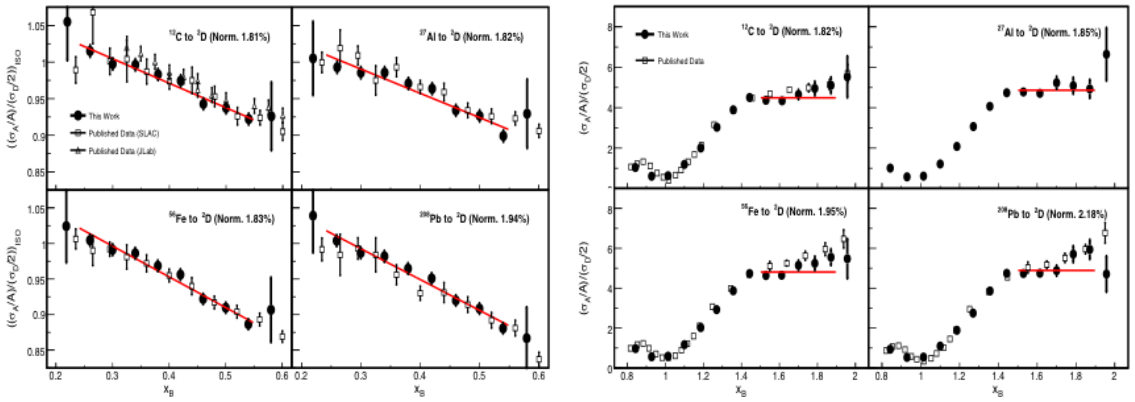

FIG. 8: New high-precision measurements of the EMC effect (left) and SRC scaling (right). See text for details.

The observation of the correlation between the strength of the EMC effect and the relative number of SRC pairs in nuclei generated new interest in the EMC effect (see CERN Courier cover paper from May 2013, Deep in the nucleus: a puzzle revisited [16]) and gave new insight into its possible origin.

A recent data-mining analysis extracted both the SRC scaling coefficients and the strength of the EMC effect for C, Al, Fe and Pb (Fig. 5) [55]. The new data were used to examine the finer aspects of the EMC-SRC correlation. Specifically, in light of the new observation of the saturation of the neutron SRC probabilities and growth of the equivalent proton probabilities (Fig. 7), it is natural to ask if the EMC effect behaves similarly for protons and neutrons. To this end, we extracted the individual per-proton and per-neutron normalized SRC scaling coefficients and EMC ratios from the (e,e') data and examined their correlation (Fig. 9). As expected from the SRC measurements, the per-neutron EMC-SRC correlation saturates starting from C, while the per-proton correlation continues to increase. This gives further support to the notion that modification of nucleons in SRC pairs is driving the EMC effect. Another implication of this observation is the existence of an isospin-dependent EMC effect: in neutron-rich nuclei, protons should be more modified on average than neutrons.

To complete the picture, we examined whether the EMC data can indeed be explained by assuming the nuclear

structure function factorizes into a collection of un-modified mean-field nucleons and modified SRC pairs, i.e.:

$$F_2^A = (Z - n_{src}^A)F_2^p + (N - n_{src}^A)F_2^n + n_{src}^A(F_2^{p*} + F_2^{n*}) \quad (1)$$

where n_{src}^A is the number of np-SRC pairs, $F_2^N(x_B)$ are the free nucleon (proton and neutron) structure functions, and $F_2^{N*}(x_B)$ are the average modified nucleon structure functions in SRC pairs. n_{src}^A is taken from experiment (i.e. from (e,e') scaling ratios at $x_B > 1$), and the modified structure function of SRC nucleons,$F_2^{N*}(x_B)$, is expected to be universal (i.e. independent of the surrounding nuclear environment).

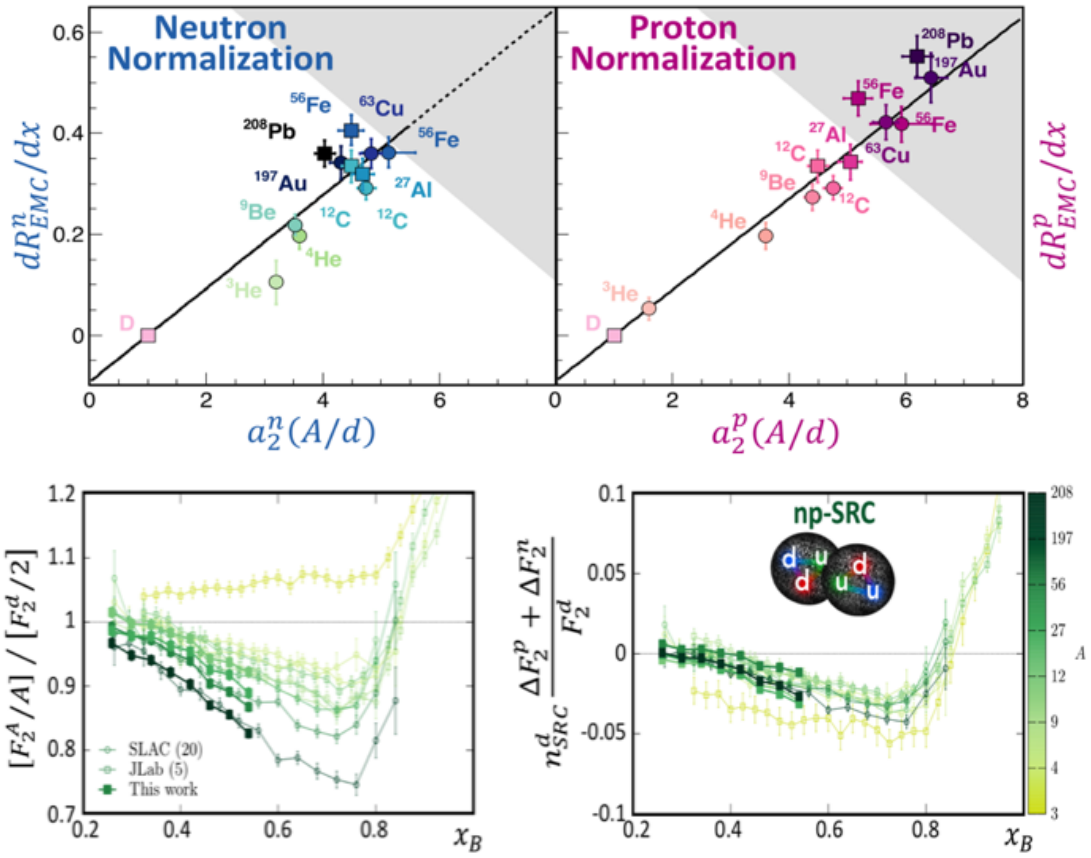

FIG. 9: Top: the EMC-SRC correlation, normalized per neutron (left) and proton (right). The saturation of the neutron correlation, starting from C, is clearly seen. Bottom left: measured structure function ratio for nuclei relative to deuterium (the EMC effect). Bottom right: extracted universal modification function of nucleons in SRC pairs.

Fig. 9 also shows the measured structure function ratios of nuclei relative to deuterium, and the extracted modification function of SRC pairs, using $\Delta F_2^N = F_2^{N*} - F_2^N$. As can be seen, while the nuclear structure functions vary significantly between different nuclei, the extracted SRC pair modification function is universal for all nuclei.

D. Summary of recent results

Hard scattering measurements of inclusive, semi-inclusive and exclusive reactions allow quantification of the properties of SRC pairs in symmetric and neutron-rich nuclei with unprecedented accuracy. The predominance of np-SRC pairs in the 300–600 MeV/c relative momentum region is observed to hold in nuclei from ^{4}He to Pb and leads to intriguing dynamics in how energy is shared between protons and neutrons in neutron-rich nuclei. Further comparisons with ab-initio and scale-separated, factorized theories show good agreement with the data. Correlations with DIS measurements of the EMC effect point to the possible impact of the detailed short-range nuclear structure on the partonic structure of bound nucleons.

However, current exclusive $A(e,e'pN)$ data are statistically limited with only several tens to hundreds of events in each measurement. The study of SRC dynamics in neutron-rich nuclei is also limited by the use of nuclei where the proton-neutron imbalance increases with mass. These limit our ability to extract information from existing data.

In addition, the discussion of the data as presented above is done within the standard QE scattering picture of the interaction. This is supported by calculations showing that the chosen kinematics of the measurements (large-Q^2, x_B >1, anti-parallel kinematics) minimize competing reaction mechanisms (e.g. meson exchange, isobar currents etc.), and allows the use of Glauber theory within a generalized Eikonal approximation to assess the impact of FSIs and guide the formation of cross-section ratios where many of these contributions are suppressed [4, 40, 43]. From a theoretical standpoint, other pictures of the interaction could exist, and one should complement and constrain reaction calculations using high statistics data spanning a wide kinematical phase-space.

III. PHYSICS GOALS

"What holds the nucleus of the atom together? In the past quarter century physicists have devoted a huge amount of experimentation and mental labor to this problem - probably more man-hours than have been given to any other scientific question in the history of mankind." -Hans Bethe, Scientific American 1953.

"However, the nuclear force is the residue of the much stronger, non-perturbative QCD force between quarks, and the fundamental nature of the short distance repulsion is not well understood in either picture." -Physics Opportunities with the 12 GeV Upgrade at Jefferson Lab, August 2012.

The existing exclusive data from $A(e,e'Np)$ and $A(e,e'pN)$ measurements, while highly instructive, is very statistically limited. This limitation becomes all the more severe in light of the significant progress made recently in ab-initio many-body theory calculations. While these first measurements could be seen as leading the field 10 years ago, at the moment, the experimental progress is lagging behind that of theory. The current proposal aims to remedy this situation by studying SRCs with unprecedented accuracy using exclusive and semi-inclusive hard scattering reactions at Hall B using CLAS12 in its standard configuration.

The proposed measurement will improve the statistics of previous studies by x10–x100. This gain in statistics will enable studies of:

1. The NN interaction and the nuclear wave function at short distances,
2. SRC pair formation mechanisms,
3. Nuclear asymmetry-dependence of SRCs,
4. Three-Nucleon SRCs,
5. The EMC Effect and its relation to SRCs.

Below, we describe each topic and how it will be addressed using the data collected in the proposed experiment.

TABLE I: Number of events collected in past SRC two-nucleon knockout measurements.

Experiment (target)	$(e,e'pp)$	$(e,e'pn)$ or $(e,e'np)$	$(e,e'nn)$
EVA/BNL (C, proton beam)	-	18 $(p,2pn)$	-
JLab E01-015 (C)	263	179	-
JLab E07-0006 (^{4}He)	50	223	-
JLab CLAS* (C, Al, Fe, Pb)	425	150	-

*Average number of events per target.

1. *NN interaction and the nuclear wave function at short distances*

Recent advances in numerical techniques, combined with the rapid development of chiral interactions, allow theorists to perform ab-initio calculations of one- and two-body nuclear densities with high precision. While these calculations are fundamental for our understanding of nuclei, and for modeling various nuclear reactions, the NN interactions used as input to such calculations, and the resulting properties of the one- and two-body densities at short distance / high-momentum lack stringent experimental constraints.

From a theoretical standpoint, a main challenge in constraining such calculations using electron scattering measurements stems from challenges in understanding the relevant electromagnetic response operators in certain kinematical regimes and a lack of data in others. These challenges will be addressed in this work in two ways:

1. **Kinematics selection and formation of cross-section ratios:** Experiments at large momentum-transfers can be calculated with high precision in a Glauber framework within a generalized Eikonal approximation. These calculations show that in the proposed kinematics for this measurement ($Q^2 > 1.5$ GeV^2, $x_B > 1$, i.e. the same as all recent measurements discussed above) the cross-section factorizes into a reaction part and a ground state part. The reaction part can be calculated, allowing constraints to be placed on the ground state part. In addition, a large part of the model-dependent reaction part cancels in cross-section ratios, such as the ones presented in Figs. 1, 2, 4. This is evident in the overall agreement of the measured cross-section ratios with ab-initio calculations shown in Figs. 1, 2, 3, 4, 7 above. To the best of our knowledge, such comparisons were not feasible until very recently. See section IV for additional details.

2. **Scale separation and factorization of ground state calculations:** In a recent publication, we showed that the generalized contact formalism discussed above allows relating experimental cross-section ratios and ground state densities via independent extractions of contact coefficients [26]. The data that will be obtained in the current proposal will be used to extract experimental contact coefficients, that will be compared with ones extracted from ab-initio calculations. Recent work (Fig. 4) extended this formalism to spectral function calculations, allowing one to not only probe integrated momentum densities but also to examine the missing energy dependence of the many-body wavefunction.

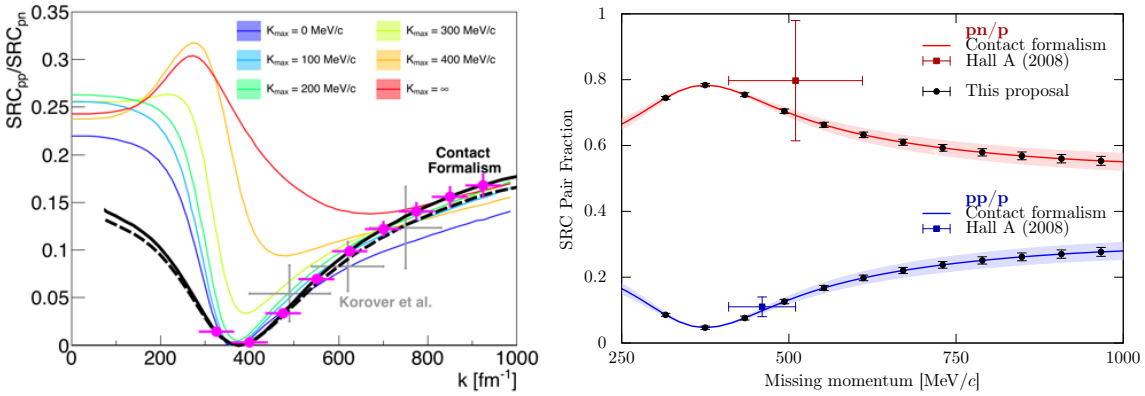

FIG. 10: projected uncertainties for the missing momentum dependence of the ^{4}He$(e,e'pp)/^4He(e,e'pn)$ (left) and C$(e,e'pn)/(e,e'p)$ and C$(e,e'pp)/(e,e'p)$ (right) cross-section ratios. The projectd data are shown as points and are compared to existing data and calculations. In the right figure the existing data is taken from a C measurement due to the very large unceratinties of the existing ^{4}He data but the new measurement will provide the relevant ratios for all measured nuclei. We expect to also extract these ratios for variou nuclei in several kinematical bins of Q^2 and $\theta_{Pmiss,q}$ to study their sensitivity to reaction mechanisms.

The high statistical yield and extended kinematical coverage of the proposed measurement will allow detailed studies of the scattering reaction and comparisons with ab-initio calculations. Fig. 10 shows an example for the expected reach in missing momentum of the new ^{4}He data as compared to existing data. The increased statistics will also allow an expanded 2-dimensional mapping in missing energy and missing momentum of the spectral function as shown in Fig. 4.

2. SRC pairs formation mechanisms

One of the crucial questions about SRC pairs is "Which nucleons combine to form the pairs?" While the short-range behavior of the pairs themselves (e.g., their relative momentum) is universal (i.e., nucleus-independent), the long-range behavior (e.g., their total momentum) depends on which nucleons form the pairs and therefore depends on the nuclear medium in which those nucleons move. Since, in one picture, SRC pairs are temporary fluctuations of two "mean-field" nucleons under the influence of the strong short-range NN interaction between them, the total (i.e., c.m.) momentum of pair will equal the total momentum of the two mean-field nucleons. The pair c.m. momentum will thus depend on which two nucleons can combine to form SRC pairs. There are many ways to select the two nucleons: any two nucleons, only nucleons in a relative s- or p- state, only nucleons in a relative s-state, only nucleons in a relative s-state and with $n = 0$, or only two nucleons at zero range. The choice of allowed nucleon states affects both how the number of NN SRC pairs changes with A (see Fig. 5), and the c.m. momentum of the NN SRC pairs

(see Fig. 6). In addition, the isospin dependence of the pairs could vary with A, leading to a different ratio of pp to pn pairs in different nuclei. Current measurements of the isospin dependence indicate that the ratio of pp to pn pairs does not vary strongly with A, although the uncertainties are large.

Current measurements are statistics limited and only measured C, Al, Fe and Pb. This experiment will increase the statistical precision of previous measurements by over an order of magnitude and will also measure many more nuclei, filling in the gaps in the A-dependence below C and between Fe and Pb. We will measure pp and pn pair abundances, and the c.m. momentum of pp SRC-pairs for the different nuclei. The increased statistics will translate to a factor of 4 decrease in the measured experimental uncertainties. By reducing the uncertainty, measurements of the pp SRC-pair c.m. momentum distribution will be able to discriminate among the different theories of pp pair formation (see Fig. 11). Similarly, improved measurements of pn and pp abundances will also be able to discriminate among the different SRC pair formation calculations, indicating precisely which pairs of nucleons are more likely to fluctuate into SRC pairs (Fig. 5). Comparisons of pp, pn and, with reduced statistics, nn pair abundances will show us whether or not the isospin dependence varies with nuclear asymmetry. In this regard, the special case of of the triplet of ^{40}Ca, ^{48}Ca, and ^{120}Sn is of patricular interest as ^{48}Ca and ^{120}Sn have the same nuclear asymetry but different mass numbers.

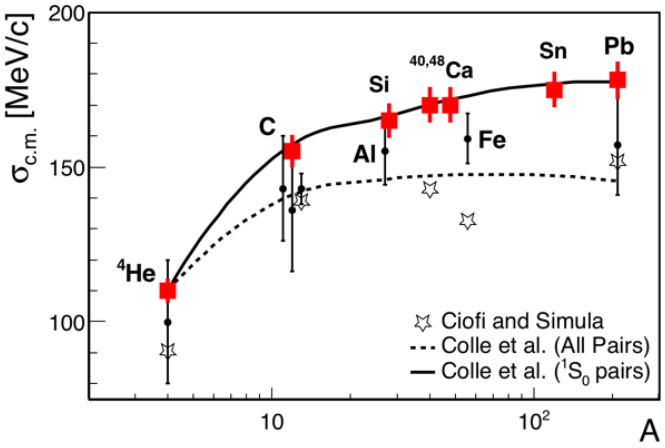

FIG. 11: projected uncertainties for the extracted width of the c.m. momentum distribution of pp- and np-SRC pairs in the measured nuclei, compared with existing data.

3. *Nuclear asymmetry dependence of SRCs*

Previous measurements show that pn pairs are the dominant component of SRC pairs for 300< p_{rel} <600 MeV/c, even in heavy asymmetric nuclei. However, because these measurements only covered C, Al, Fe and Pb, they could not disentangle the effects of increasing the nuclear mass from increasing the nuclear asymmetry. In this proposal, we will cover more nuclei with higher statistical precision, and we will disentangle mass number from asymmetry. This will be done by constraining the mass dependence from measurements on a series of symmetric nuclei (d, ^{4}He, C, Si, ^{40}Ca) and then focusing on asymmetry dependence from ^{48}Ca, ^{120}Sn and ^{208}Pb. As mentioned above Ca and Sn complement each other on asymetry and varie in mass which will also help disentangle the two dependencies.

We will repeat the $A(e,e'p)$ and $A(e,e'n)$ measurements shown in Fig. 7 for more nuclei, including ^{40}Ca, ^{48}Ca and ^{120}Sn, and with much greater statistical precision. By including the calcium isotopes and tin in the measurement, we will test the observed N/Z dependence of the $(e,e'n)/(e,e'p)$ low-missing-momentum ratio and the observed A independence of the $(e,e'n)/(e,e'p)$ high-missing-momentum ratio. We can also test how the high-missing-momentum fraction of $(e,e'n)$ and $(e,e'p)$ events changes when we vary mass number and neutron excess independently.

Similar studies will be done using the exclusive $(e,e'NN)$ reactions that will yield further insight to the mass and asymetry dependence of specific pairs isospin states. Combined with the increased statistical precision of the measurement will allow the refinement of our crude empirical (yet useful) np-dominance model, such as the inclusion of the known few-percent abundances of pp and nn SRC pairs.

4. Three-Nucleon SRCs

Once the existence and properties of Two-Nucleon (2N) SRCs are established, it is natural to search for Three-Nucleon (3N) SRCs. The available beam energy, detectors and luminosity limited the reach of exclusive measurements done at Halls A and B in searching for 3N-SRCs.

Searches for 3N-SRCs using inclusive (e, e') measurements at $x_B > 2$ kinematics during the JLab 6 GeV era were largely unsuccessful, either due to resolution issues [11, 56], or due to the required Q^2 reach [57]. It is unclear at the moment if the high-Q^2 required by inclusive measurements ($\sim$4–6 GeV^2) can be reached in $x_B > 2$ kinematics even using a 12 GeV beam [58]. On the other hand, in exclusive reactions, the added information obtained from the detection of the leading and recoil nucleons should provide the required reach, even at lower Q^2 and x_B.

From a theoretical standpoint, there is much to learn about 3N-SRCs (see recent review in [58]). One model describes the creation of triples as the result of a subsequent short-ranged tensor interaction which is effectively described as two 2N-SRC interactions [59]. This predicts that the 3N-SRC probability will equal the 2N-SRC probability squared, giving them a very different nuclear mass- and asymmetry-dependence compared with $2N$-SRCs. In addition, such a mechanism implies that the three nucleons are co-linear, with one very high-momentum nucleon balanced by two lower momentum nucleons moving in the opposite direction. Other models describe 3N-SRC using irreducible 3N forces that lead to three nucleons with similar momenta oriented in a star configuration with a significantly different nuclear mass- and asymmetry-dependence.

At the moment, the only available exclusive data come from a preliminary analysis of $(e, e'ppp)$ and $(e, e'npp)$ reactions from CLAS6. These have several 10s of events and seem to support the "star configuration" hypothesis. However, the available statistics and kinematical coverage are not enough to make a definitive claim and to establish a direct observation over other reaction mechanisms.

Utilizing the increased CLAS12 luminosity and improved neutron detection capabilities, the proposed measurement will be sensitive to 3N-SRC in several exclusive reaction channels such as $(e, e'ppp)$ and $(e, e'npp)$. We extimate a measure of 200 to 2,000 such events, depending on the reaction (see Table IV below), which is comparable to, or higher than, the 2N-SRC statistics that yielded the results presented in section II above (see Table I).

5. Reaction mechanisms (QE nucleon knockout)

There is regrettably no conclusive way to know, from the measurement of the final-state particles, which reaction mechanisms were involved in any particular event. The reaction could include contributions from direct knockout of a nucleon (QE, the desired reaction mechanism), or from Meson-Exchange Currents (MEC), Isobar Currents (exciting the struck nucleon to an excited state, IC), and elastic and inelastic nucleon rescattering (final-state interactions or FSI). In the case of high missing momentum, elastic FSI can include re-scattering between the nucleons of the pair and/or with the residual system. The relative contribution of these reaction mechanisms, as compared to the QE reaction of interest, strongly depends on the reaction kinematics [2–4, 41, 43]. Minimizing non-QE reaction mechanisms also reduces their interference with the QE reaction.

The high-missing-momentum measurement proposed here will be carried out in high-Q^2, $x_B > 1$, largely anti-parallel kinematics. This kinematical region minimizes non-QE reaction mechanisms as follows [2, 4, 5, 41]: (A) MEC are suppressed by a factor of $1/Q^2$ compared to QE, are further suppressed at $x_B > 1$, and their contribution in our kinematics is small. (B) IC are also suppressed at $x_B > 1$ where the energy transfer is relatively smaller, and (C) at large knockout nucleon momenta we can reliably calculate FSI effects using a generalized Eikonal approximation in a Glauber framework. These calculations show that in these kinematics, elastic FSI are largely suppressed for mean-field nucleon knockout. For SRC breakup, FSI are confined to the two close-proximity nucleons in the SRC pair [4, 43]. Additional discussion of the validity of the Glauber approximation in the relevant high-Q^2 kinematics is given in [4, 31, 40, 41, 45].

A strong support for the use of the simple QE picture, with suppressed FSI, is the fact that it describes well both high-Q^2 electron scattering data as well as high energy proton scattering data taken at BNL [8, 9]. With very different reaction mechanisms, the results of the high momentum transfer ^{12}C$(p, 2p)$ and ^{12}C$(p, 2pn)$ measurements are in full agreement with the high-Q^2 electron scattering data as evident in the isospin ratio of SRC pairs [5] as well as their center of mass momentum distributions [9, 37]. However, this agreement is statistically limited.

The anticipated high statistics of the proposed measurement should allow for detailed tests of the reaction mechanisms. First and foremost, we would test the expected Q^2 independence of the extracted one- and two-nucleon knockout cross-section ratios. Theory calculations of the reaction mechanism at the measured $x > 1$ anti-parallel kinematics predict that at high-Q^2 (> 1.5 GeV^2) the measured cross-section ratios will be Q^2-independent up to very large values of Q^2 where effects of Color-Transparency might appear.

In addition, for a given Q^2, the calculations described above also show significant dependence of FSI on the relative angular orientation between the missing momentum and the virtual photon. SRC measurements are done in anti-parallel kinematics to minimize FSI. While these calculations have been verified for the deuteron, we do not have enough statistics for heavier nuclei. The high-statistics data obtained in this measurement will be used to test these calculations via the angular and A-dependence of the measured cross-sections and cross-section ratios.

This measurement will span a wide momentum transfer range of ∼0.5–5.5 GeV^2, providing stringent tests for reaction mechanism calculations.

6. EMC Effect and its relation to SRCs

As mentioned above, our recent observation of a linear correlation between the size of the EMC effect and the relative number of SRC pairs in nuclei brought new insight to the possible origin of the EMC effect. This observation naturally led to the development of several theoretical models relating the EMC effect to the modification of the internal structure of high-virtuality nucleons, suppression of point-like configurations (PLCs) and others (see review in [1]). An extensive experimental program is approved to test these models. The proposed measurement will provide a unique test of this by extracting the per-nucleon ratios of the DIS cross-sections on nucleus A compared to the deuteron as a function of x_B, tagged by the detection of a high-momentum recoil proton or neutron in the backward hemisphere (tagged EMC ratios). If, as we expect, the EMC effect is predominantly associated with nucleons in SRC pairs, and SRC pairs are the leading source of high-momentum recoil nucleons, then this ratio will be flat with a deuteron-like momentum distribution for the recoiling nucleons. This is true also for the tagged QE ratios that are flat over a much wider range in x_B than the standard (untagged) inclusive QE ratios (see preliminary results in Fig. 12). Using the CLAS12 detector, we will also be able to tag recoil neutrons, especially using the new BAND detector that is expected to be installed this summer. The CLAS12 central detector detects neutrons at scattering angles up to about 135° with an efficiency of 10%, while the BAND detector will detect neutrons at much more backward scattering angles from 160 to 170° with an efficiency of about 40%.

Therefore, by comparing inclusive and tagged QE and DIS scattering off deuterium, light and heavy nuclei we will be able to test the finer details of SRC dynamics and the EMC effect and gain additional insight as to their possible common origin. The addition of the BAND detector will significantly increase the CLAS12 recoil neutron acceptance in the crucial back-angle region, allowing for unique tests of isospin asymmetry.

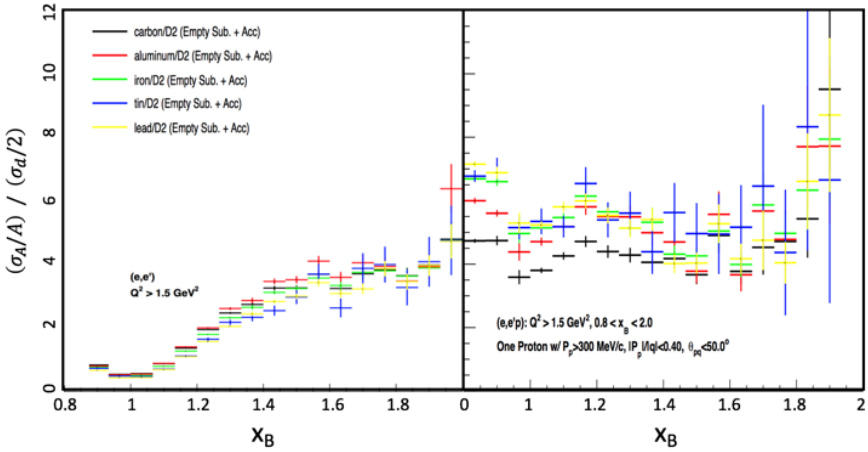

FIG. 12: Preliminary x_B dependence of the (e, e') (left) and (e, ep_{recoil}) (right) cross-section ratios for nuclei relative to deuterium for $< Q2 >\sim 2$ GeV^2. The new measurements will have improved statistics and neutron detection capabilities over a wider range of nuclei.

IV. PROPOSED MEASUREMENT I: KINEMATICS AND EVENT SELECTION

A. $A(e,e'p)$ formalism at High-Q^2

The cross-section for electron-induced proton knockout from nuclei $A(e,e'p)$ can be written (assuming factorization) as:

$$\frac{d^6\sigma}{d\nu dE_{miss} d\Omega_e d\Omega_p} = K\sigma_{ep} S^D(E_{miss}, p_{miss})$$

where σ_{ep} is the cross-section for scattering an electron from a bound proton. The missing energy and missing momentum are:

$$E_{miss} = \omega - KE_p - KE_{A-1} \quad (2)$$
$$\vec{P}_{miss} = \vec{q} - \vec{P}_p \quad (3)$$

where KE_p and KE_{A-1} are the kinetic energies of the outgoing proton and residual nucleus, the momentum transfer $\vec{q} = \vec{P}_e - \vec{P'}_{e'}$, $S^D(E_{miss}, p_{miss})$ is the distorted spectral function and the kinematical factor is K

$$K = \frac{E_p P_p}{(2\pi)^3}.$$

In the absence of final state interactions (FSI), S is the nuclear spectral function that defines the probability to find a nucleon in the nucleus with separation energy E_{miss} and momentum p_{miss} [60]. The energy transfer is $\omega = E - E'$ where E and E' are the initial and scattered electron energies. The $\vec{P}_e$ and $\vec{P'}_{e'}$ are the initial and scattered electron momenta, $\vec{P}_p$ is the outgoing proton momentum, and Ω_e and Ω_p are the electron and proton solid angles respectively. The angle between the recoil momentum and $\vec{q}$ is called $\theta_{recoil,q}$. As detailed below, we will restrict $\theta_{recoil,q}$ to minimize final state interactions.

B. Reaction mechanisms and event selection

To identify events where the electron scattered from a pn or pp SRC pair that is in the nuclear ground state, we work in a kinematic regime in which competing processes are suppressed. Such processes include: Meson Exchange Currents (MEC), Isobar Configurations (IC), and Final State Interactions (FSI).

Fig. 13 shows the different Feynman diagrams associated with these reaction channels. In the figure, the bottom left diagram describes FSI between the nucleons in the SRC pair, and the bottom right diagram describes FSI with the $A-2$ system. Notice that the FSI within the SRC pair conserves its nucleonic composition (i.e. pp, nn, np, etc.) and c.m. momentum. In what follows (except if mentioned otherwise) FSI refers to the process described in the bottom right diagram.

First, we choose to work in scattered electron kinematics corresponding to high-Q^2 and $x_B > 1$. This is motivated by the fact that the MEC diagram amplitude decreases faster than the SRC one by a factor of $1/Q^2$. Additionally, for a given Q^2, IC are suppressed in the $x_B = Q^2/(2m_p\omega) > 1$ region. An added advantage of measuring at large Q^2 is that the struck (leading) proton has high momentum, allowing the use of the Glauber approximation to evaluate the contributions of FSIs.

There are two general effects from the rescattering of the outgoing nucleon: a shift in its momentum due to the real part of the proton-nucleus potential and rescattering of the proton that changes its momentum and potentially knocks out a second nucleon. At high-Q^2, these FSI effects primarily include Nuclear Transparency, the probability that a knocked-out nucleon is scattered out of our acceptance, and SCX, the probability that a struck neutron elastically scatters off a proton on its way out of the nucleus leading to the detection of the proton in the final state and vise-versa. Details of these effects are described in [4, 6].

The consideration for nucleons that rescatter into a particular kinematic bin relays on our knowledge that it is maximal at perpendicular kinematics, where the angle between the recoil momentum and the momentum transfer, $\theta_{recoil,q} \approx 70°$. This happens because most collisions between high-momentum protons and other nucleons in the nucleus deflect the high-momentum only slightly, kicking the struck nucleon out at about 70° (non-relativistically it would be about 90°). This can be seen clearly in calculations of the data of [62], where the cross-section at $p_{miss} > 250$ MeV/c and $E_{miss} \approx p^2_{miss}/2m$ is due almost entirely to rescattering. This is supported by ^{3}He$(e,e'p)$ calculations [61] that show very large contributions due to proton rescattering peaked at $\theta_{recoil,q} \approx 70°$. In order to avoid these regions where rescattering is much larger than the SRC signal, we will choose to further restrict the $A(e,e'p)$ kinematics to small angles between the momentum transfer and the recoil momentum, $\theta_{recoil,q} \leq 40°$.

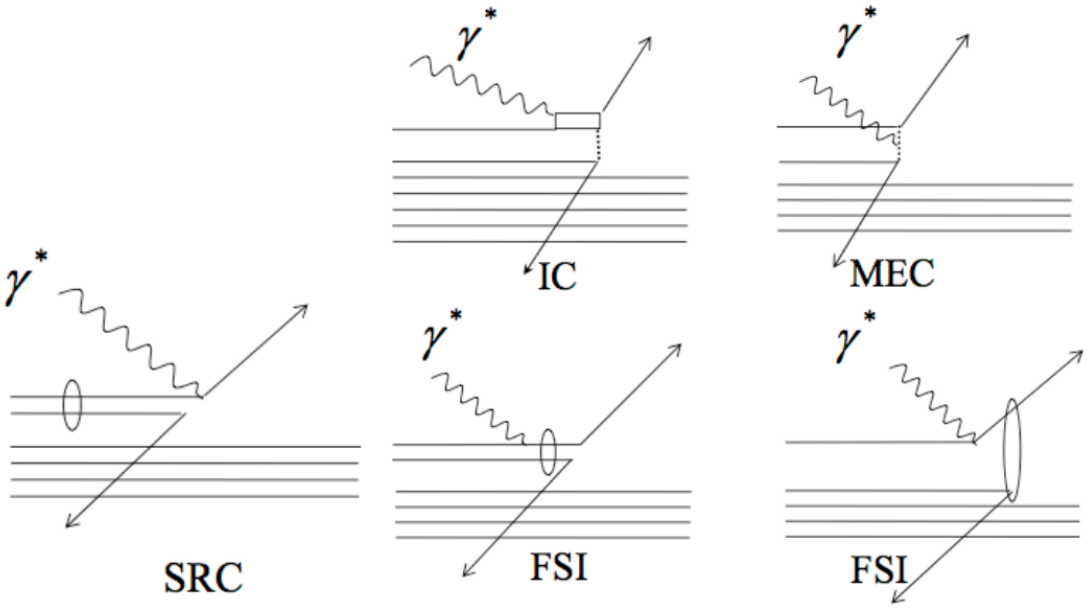

FIG. 13: Feynman diagrams of the different possible reaction channels, leading to a two-nucleon final state. The γ^* indicates the virtual photon that carries the momentum and energy transferred from the electron to the proton. The double line indicates an excited state of the proton, the dashed line indicates a meson, and the ellipse indicates an interaction between two nucleons. The difference between the two FSI diagrams shown is that one entails FSI between the nucleons of the pair (left diagram) and the other FSI of uncorrelated nucleons (right diagram). [6]

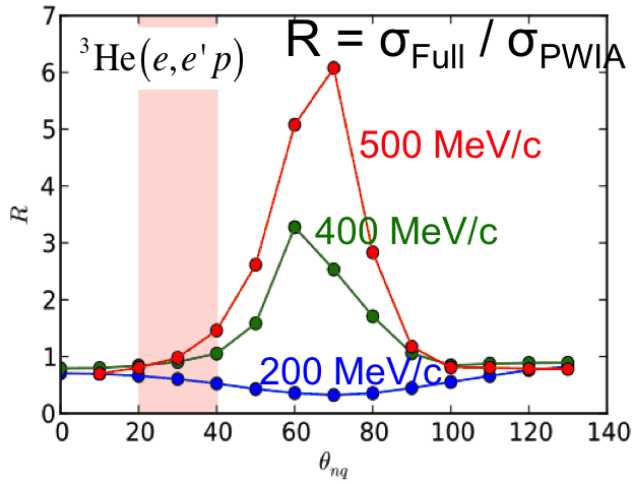

FIG. 14: The calculated ^{3}He$(e,e'p)$ ratio of the cross-section which includes rescattering of the struck nucleon (FSI) to the PWIA cross-section for $p_{miss} = 0.2$ (blue), 0.4 (green), and 0.5 (red) GeV/c as a function of $\theta_{recoil,q}$, the angle between the recoil momentum and $\vec{q}$ in the laboratory frame [61].

Therefore, to simultaneously minimize both FSI, MEC and IC, we choose $x_B > 1$, large-Q^2, anti-parallel kinematics, in which the initial momentum of the struck proton is directed opposite (anti-parallel) to the virtual photon (i.e., to the transferred momentum). In such kinematics, after absorbing the virtual photon, the struck proton is emitted in the same direction as the virtual photon but with smaller momentum. This corresponds to the following $A(e,e'N)$ event selection cuts [6, 31]:

1. x_B >1.2
2. 300 <| p_{miss} |< 1000 MeV/c

3. $\theta_{pq} < 25°$
4. $0.6 < |\vec{P}| / |\vec{q}| < 0.96$
5. $m_{miss} < 1.1$ GeV/c

We define $\vec{P}_{miss} = \vec{P} - \vec{q}$ as the reconstructed initial (missing) momentum of the leading detected nucleon. The reconstructed missing mass, m_{miss}, is defined as $m^2_{miss} = [(\vec{q}, \omega) + (\vec{0}, m_d) - (\vec{P}, E_p)]^2$ where ω is the energy transfer, m_d is the deuteron mass, and $\vec{P}$ and E_p refers to the momentum and energy of the lead detected proton, respectively. These above-listed cuts ensure that we are selecting a sufficiently high Q^2 (i.e. > 1.5 GeV/c^2). Cutting on p_{miss} selects scattering off high initial-momentum nucleons. Cuts on $\vec{P}$ select the lead proton of the reaction. A cut on the m_{miss} suppresses pion production and the isobar contribution. Nucleons knocked out of the nucleus with high momentum and a small angle with respect to the momentum transfer $\vec{q}$, are more likely to be the ones struck by the virtual photon.

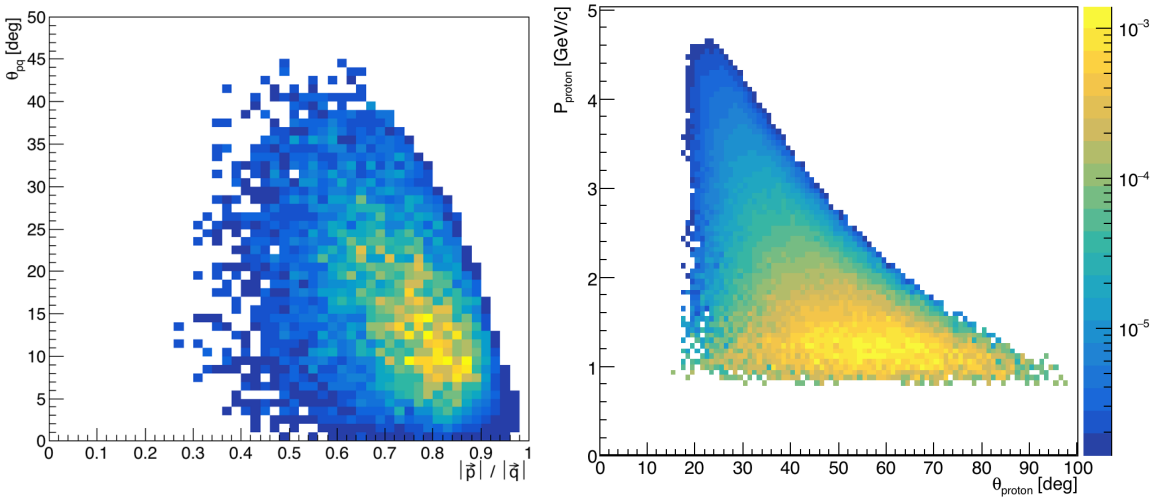

FIG. 15: Here we select events with $x_B > 1.2$ and $Q^2 > 1.5$ GeV^2. Left: The ratio of the magnitudes of the lead proton momentum to the momentum transfer. The lead proton is knocked out at small angles relative to $\vec{q}$ ($< 25°$) and carries a large fraction of the momentum transfer. Right: After selecting the lead proton, the angular and momentum distributions of the lead proton are shown.

Fig. 15 (left) shows the relative angle between the virtual photon and the detected proton θ_{pq} versus the ratio between the detected proton momentum and the momentum transfer, from a dedicated SRC kinematical simulation. The lead proton is knocked out at small angles relative to $\vec{q}$ ($< 25°$) and carries a large fraction of the momentum transfer. After selecting the lead proton for the relevant kinematics, we observe the recoil particle emitted back-to-back with respect to the missing momentum vector. In Fig. 16, we see that the recoil particle and the missing momentum are emitted at anti-parallel kinematics up to approximately 40°. By measuring events with $\theta_{recoil,q}$ at angles less than 40°, we significantly reduce contamination from nucleon re-scattering.

In the absence of FSI, the angle between the recoil particle and the lead detected proton is the angle between the two particles in their initial state in the nucleus. The width of the distribution of this angle is smeared by the c.m. motion of the nucleon pair. While FSI increase with the nucleus A, the true measured width of the c.m. motion of the nucleon pair has been shown previously to be the same across all nuclei [6].

On the right of Fig. 16, we observe the kinematical distribution of the recoil particle, which could be a proton or neutron. We look for recoil particles with a momentum between 350 MeV/c and 1 GeV/c. With the CLAS12 detector, this experiment will be able to measure some recoil particles in $A(e, e'pN)$ reactions. $A(e, e'pN)$ events are defined as $A(e, e'p)$ events with the detection of the recoil particle.

C. Measured observables

This experiment will measure exclusive and semi-inclusive hard scattering reactions on ^{2}H, ^{4}He, C, Si, ^{40,48}Ca, Sn, and Pb targets to probe short range pairing mechanisms. The chosen target nuclei have several features that make them of interest to this experiment, for example:

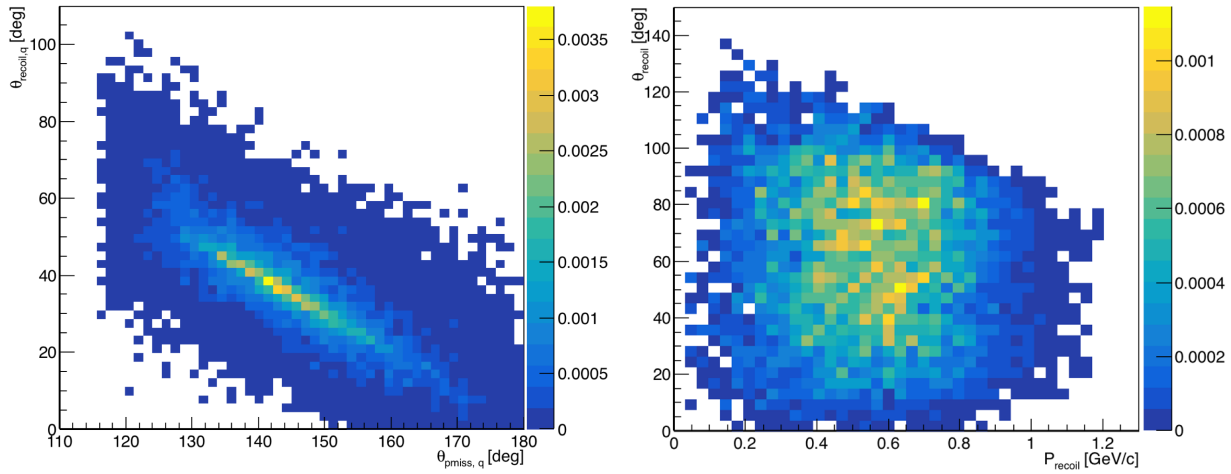

FIG. 16: Here we select events with $x_B > 1.2$ and $Q^2 > 1.5$ GeV^2 with the selection of the lead proton cuts as described previously. Left: The angle $\theta_{pmiss,q}$ is the angle between the missing momentum $\vec{P}_{miss}$ and momentum transfer $\vec{q}$, and the angle $\theta_{recoil,q}$ is the angle between the recoiled particle momentum $\vec{P}_{recoil}$ and the momentum transfer. We see that the recoil and missing momentum are anti-parallel with respect to each other. Right: The recoil particle is emitted at angles that predominantly occupy the central part of the CLAS12 detector up to momentum of 1 GeV/c.

- ^{2}H is the simplest *np* system that shows scaling in ratios to SRC measurements in heavier nuclei and therefore commonly serves as a reference system,
- ^{4}He features many of the complexities of the nuclear many-body problem (e.g. 10% - 15% SRC pairs, including all isospin combinations) but is very light so reaction mechanisms are relatively small and exact calculations are feasible,
- ^{2}H, ^{4}He, C, Si, and ^{40}Ca are symmetric nuclei that vary in mass number, which allows probing the mass dependence of SRCs and also getting a better handle of reaction mechanism effects for studies of SRCs in neutron-rich nuclei,
- ^{40}Ca and ^{48}Ca are doubly-magic isotopes, with ^{48}Ca having a 40% neutron excess which allows studying nuclear asymmetry effects in a systematic manner,
- ^{48}Ca and ^{120}Sn both have the same neutron excess but different mass numbers, allowing to better decouple mass and asymmetry dependencies,
- Pb is the heaviest and most neutron-rich nucleus available for measurements.

For each nucleus, we will measure across the full range of p_{miss} kinematics up to 1 GeV/c. We will extract the cross-section ratios, such as $A(e,e'pn)/A(e,e'pp)$, $A(e,e'pp)/A(e,e'nn)$, $A(e,e'p)/C(e,e'p)$ and $A(e,e'pN)/C(e,e'pN)$ and calculate the double ratio as $[A(e,e'p)/C(e,e'p)]$ $/[A(e,e'pN)/C(e,e'pN)]$, where, for specific cases, C will be replaced by ^{40}Ca or any other nucleus of interest. By taking the double ratio, overall normalizations and corrections cancel. This technique was used previously in the EG2 experiment, see Fig. 7 discussion in [32].

We will extract reduced cross-sections for all possible one, two, and three nucleon knockout reactions in the measured nuclei which will allow us to learn about SRCs by extracting ratios of:

- *np*- *nn*- and *pp*- SRC pairs in each measured nucleus and in one nucleus relative to another,
- high to low momentum protons in each measured nucleus,
- high-momentum protons in heavier nuclei to deuterium and to the closest symmetric nucleus,
- double ratios of high to low momentum protons in heavier nuclei and to the closest symmetric nucleus,
- double ratios of 2N-SRC ratios to 3N-SRC ratios,
- DIS ratios tagged with high-momentum recoil nucleons.

In addition, we will study the c.m. motion of $2N$ and $3N$-SRC pairs, where the latter will be part of a broader search for three-nucleon correlation in exclusive reactions that will also include forming ratios of three-nucleon knockout reactions in a given nucleus to study their isospin structure and between different nuclei to study their A-dependence [59].

We note that we will need to correct each of these for the effects of final state interactions (FSI), as done in previous works. The high-luminosity and large kinematical coverage of CLAS12 will allow us to study these correlations by examining the Q^2 and $\theta_{recoil,q}$ of the various ratios.

V. PROPOSED MEASUREMENT II: EXPERIMENTAL SETUP AND EXPECTED EVENT COUNT RATE

We propose to extend SRC measurements in nuclei by covering a wider range of nuclei and enhancing the statistics, especially for measurements of $A(e,e'Np_{recoil})$ and $A(e,e'pN_{recoil})$ where we have been historically limited. We will use the large-acceptance, open (i.e., electron only) trigger, and enhanced neutron detection of the CLAS12 detector to measure exclusive and semi-inclusive hard scattering from a variety of targets. The extra layers of the forward electromagnetic calorimeter and the central neutron detector as well as the BAND detector, will significantly enhance our ability to detect neutrons in these events.

A. Experimental setup and kinematical coverage

We plan to measure scattering on ^{2}H, ^{4}He, C, Si, ^{40,48}Ca, Sn, and Pb targets at incident beam energies of 4.4 and 6.6 GeV. These targets span a large range of nuclei and expand on the previous measurements during the 6 GeV era, with higher statistics.

We will use a new CLAS12 liquid and solid target system, currently under development by W. Brooks, H. Hakobyan and I. Vega at the Universidad Tecnica Federico Santa Maria (UTFSM) for approved experiment E12-06-117. This system consists of a 5 cm long liquid target cell and a set of solid targets attached to a movable tape system at the downstream end (Fig. 17). The target system has already been designed and tested and will be ready for use in 2019. This target-system should be able to support all targets of interest, except for ^{40}Ca and ^{48}Ca that require encapsulation and will, therefore, need to be mounted separately.

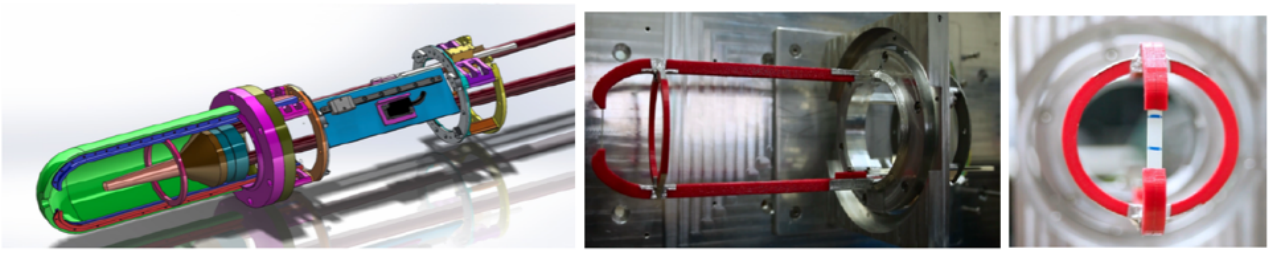

FIG. 17: The CLAS12 target system developed at UTFSM. (left) A drawing of the system showing the target vacuum enclosure (green), the tapering liquid target cell (copper), and the upper (blue) and lower (red) supports for the solid target tape; (middle) the prototype solid target system with the upper and lower supports (red). The tape with the solid targets passes between the upper and lower supports at the far left; (right) end view looking upstream at the tape with the solid targets.

CLAS12 will be used in its standard configuration and an in-bending field configuration. Compared to CLAS6, CLAS12 has several advantages with respect to exclusive SRC studies:

1. **Operational luminosity:** CLAS12 can measure luminosities higher by x10 than CLAS6.

2. **Recoil nucleon acceptance:** while the CLAS6 azimuthal acceptance averaged 50%, the CLAS12 central detector has almost full azimuthal acceptance.

3. **Neutron detection:** high-momentum (leading) neutrons can be detected using the CLAS electromagnetic calorimeters and low-momentum (recoil) neutrons can be detected in the CLAS forward FTOF scintillators (at $\theta_n < 40°$) or the Central Neutron Detector (CND). CLAS6 had a single EM calorimeter with 30-50% neutron detection efficiency and one 5 cm-thick scintillator layer for TOF measurements with 3-6% neutron detection efficiency. CLAS12 has an added pre-shower calorimeter which increases the high-energy neutron

detection efficiency. The forward TOF scintillators are double layered which doubles their neutron detection efficiency, and the CLAS12 central-detector includes a neutron detector with excellent TOF resolution and a ∼10% detection efficiency. Some of the spokespersons of this proposal are also building a back-angle neutron detector (BAND) with 40% detection efficiency to be installed in late 2018.

These technical improvements allow increasing the statistics of the measurement of charged particles by about 20–40 times for the same beam time (see details below) and open additional neutron detection channels, including $(e, e'nn)$ whose comparison with $(e, e'pp)$ in asymmetric nuclei is of vast interest.

The main challenge of using CLAS12 for QE scattering measurements is its momentum reconstruction resolution. The missing momentum resolution depends on the reconstructed resolution of the scattered electron and knocked-out (leading) proton and is a key consideration for the design of the proposed experiment. Simulation studies done for this proposal using GEMC and standard CLAS12 reconstruction software show that the momentum resolution for scattered electrons in the 10° – 20° angular range is largely independent of the scattered electron momentum and equals ∼0.4% (Fig. 18).

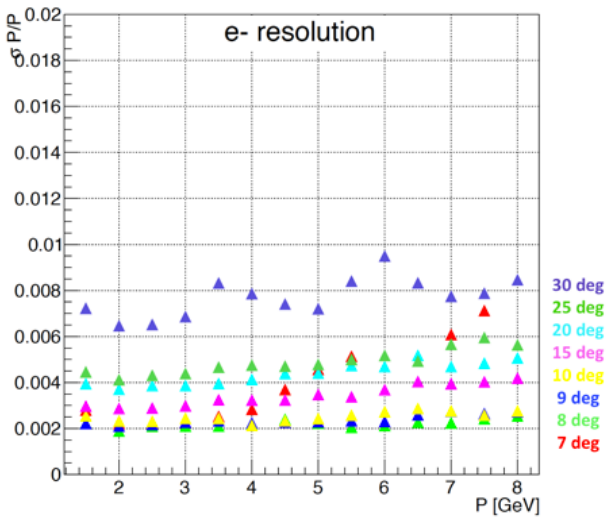

FIG. 18: The electron momentum resolution in an in-bending toroidal field is shown where the various angles in the generated theta angle are shown, separately. For most events of interest to SRC at 6.6 GeV, we expect approximately 0.4% resolution of the electron.

This agrees with previous studies of the CLAS12 resolution. While this reconstruction resolution is similar (and even slightly better) to that of CLAS6, the use of a higher-energy incident electron beam will reduce the reconstruction resolution of the momentum transfer vector and therefore of the missing momentum. For a 10.8 GeV beam, the scattered electron energy in QE kinematics is ∼10 GeV which leads to resolution of 40 MeV/c (before accounting for the contribution of the proton reconstruction to the missing momentum), which is too large for the purposes of the current proposal. We therefore choose to use a 6.6 GeV beam, for which the scattered electron energy is ∼5.7 GeV which leads to a resolution of 27 MeV/c. The addition of measurements going down to a 4.4 GeV beam will improve the resolution by 5 MeV/c and allow for an extended kinematical dependence study, but have a reduced count rate by about 40% due to the reduced Mott cross-section for a given x and Q^2.

Estimating the impact of the leading proton momentum reconstruction on the missing momentum is more complicated, as it covers a wider momentum and angular range. For a given x and Q^2, the leading proton momentum has very little dependence on the beam energy. However, its scattering angle does depend on the exact kinematics which will impact the relative fraction of leading protons detected by the forward vs. central detector. This is especially important for studies of neutron knockout reactions as high-momentum neutrons can only be detected in the caloremeters of the CLAS12 forward detector.

To study this we developed a dedicated SRC event generator that allows studying the kinematics of the proposed measurement. The generator was implemented for use in GEMC with the current CLAS12 detector model so that the CLAS12 acceptance and reconstruction capabilities could be studied. SRC events were reconstructed over a wide measurement phase-space (Fig. 19).

From the simulations, we studied the resolution for reconstructing the leading proton as this resolution directly impacts our missing momentum resolution. The reconstructed leading proton resolution is shown in Fig. 20.

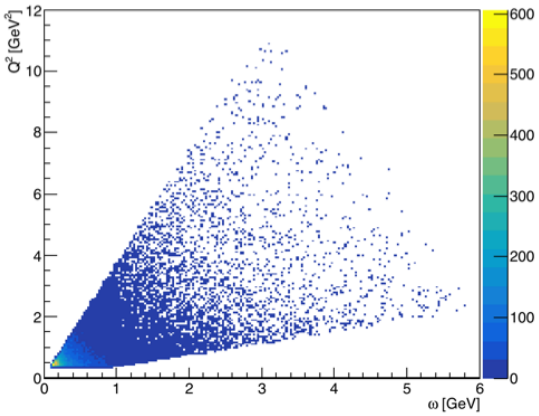

FIG. 19: Momentum transfer Q^2 versus the energy transfer ω for a 6.6 GeV incident beam.

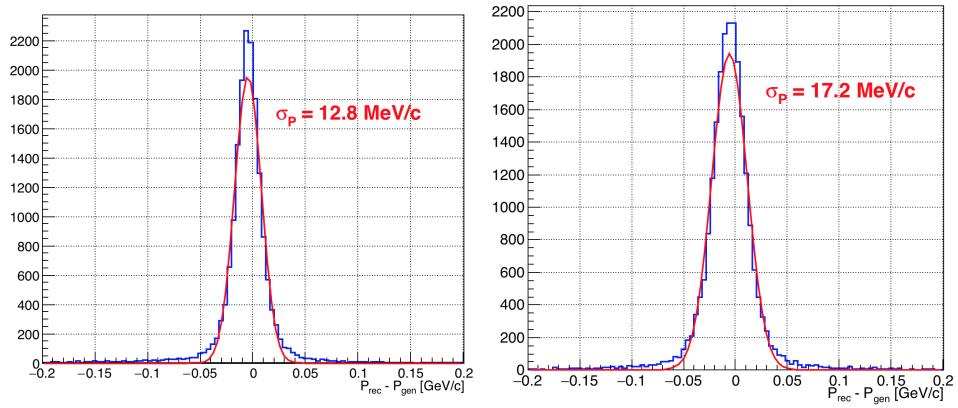

FIG. 20: From GEMC simulation of short range correlation kinematics, we selected the lead proton where $x > 1.1$ and $Q^2 > 1.5$ GeV^2. Left (right) shows the lead proton reconstructed resolution for a 4.4 (6.6) GeV beam. For a 6.6 GeV beam, the resolution of the lead proton is approximately 17 MeV/c which yields a missing momentum resolution of approximately 30 MeV/c. The 4.4 GeV beam yields a slightly better proton resolution, as anticipated.

We expect that a 6.6 GeV beam energy will yield a total missing momentum resolution better than 30 MeV/c. This is comparable to what was obtained in CLAS6 and is sufficient for SRC physics. The 4.4 GeV running improves this by a few MeV/c as shown on the left in Fig. 20.

We observe that protons detected in the forward detector of CLAS12, have a better reconstructed resolution than those captured in the central detector. This is significant for high-momentum protons (> 1.5–2 GeV/c) from high-Q^2 events. By moving the target position downstream, we are also able to measure more protons from our kinematics of interest in the forward detector. While it is possible to move the target as far as 20 cm downstream, we conservatively simulated the target positions from target center to 15 cm downstream and observed the improved proton acceptance in the forward detector with the target further downstream. The higher Q^2 events, corresponding to larger proton momenta that are preferably going into the forward detector (see Fig. 21) where θ, with respect to target center, is less than 40°. Because these protons have an improved reconstructed momentum resolution from being detected in the forward detector, they produce a comparable missing momentum resolution.

Generated events were reconstructed using the standard CLAS12 reconstruction framework. The reconstructed lead proton is shown on the left in Fig. 22. The missing momentum was reconstructed using the lead proton and scattered electron. The residual missing momentum for 6.6 GeV kinematics is shown on the right of Fig. 22 with a slightly narrower width than anticipated due to small momentum shifts in the current reconstruction.

For completeness, in the case of DIS studies it is instructive to examine the (e, e') acceptance in terms of W and Q^2. This is shown in Fig. 23 for a 6.6 GeV beam and the CLAS12 acceptance. As can be seen, hard DIS coverage ($W > 1.8$ GeV and $Q^2 > 1.5$ GeV^2) extends up to $x \sim 0.7$, which covers the full EMC region of interest. This is a large improvement over the CLAS6 acceptance that reached only up to $x \sim 0.55$.

A second potential issue that we studied is the impact of the increased CLAS12 luminosity on the measured random-coincidence background in neutron detection channels. While the signal rate scales linearly with luminosity,

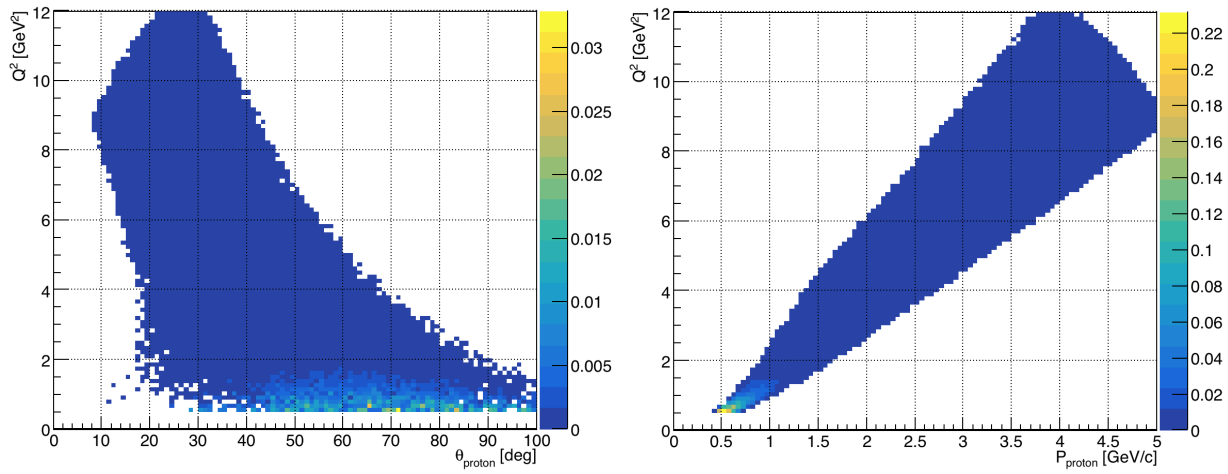

FIG. 21: From the event generator characterizing SRC kinematics, we show spectrum of generated protons at $x > 1.1$. These protons correspond to the reconstructed lead proton. Higher Q^2 lead protons in our kinematics will tend toward more forward angles and higher momenta.

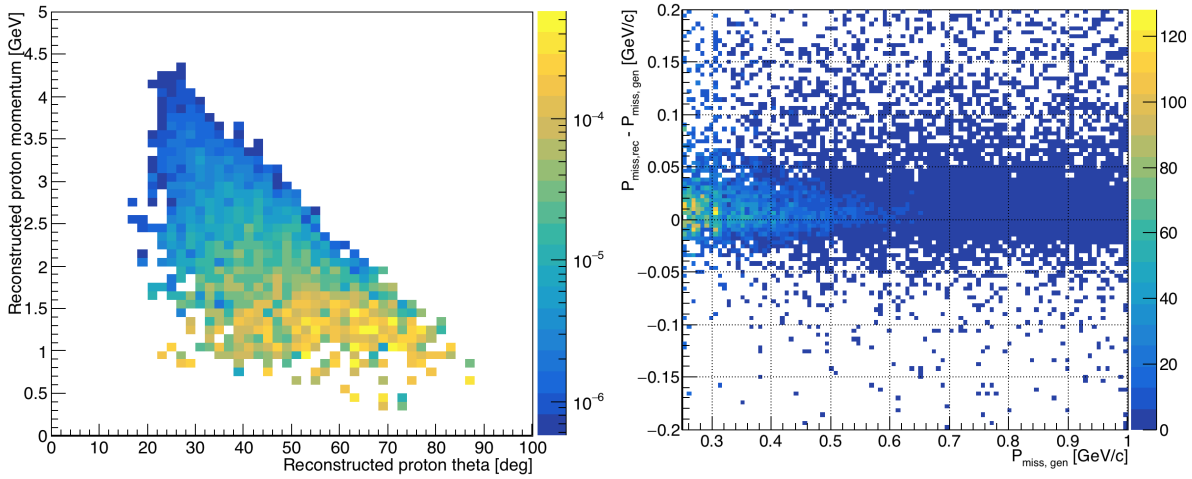

FIG. 22: SRC simulations in the GEMC CLAS12 implementation using the standard CLAS12 reconstruction software package. On the left, we see the reconstructed proton momentum versus the angle θ in the CLAS12 detector. Most events we reconstruct are in the central region ($> 40^\circ$) of the detector. On the right, we reconstruct the missing momentum from the proton and electron and plot the residual. The width of the reconstructed missing momentum from simulation is slightly better than the anticipated 30 MeV/c obtained from the quadratic sum of the electron and proton contributions due to small shifts in the current implementation of the CLAS12 software.

the random coincidence background (BG) is given by: $R_{BG} = R_{e-singles} \cdot R_{n-singles} \cdot \Delta t$, where R_{BG} is the random coincidence rate, $R_{e-singles}$ and $R_{n-singles}$ are the singles electron and neutron hits rates and $\Delta t = c \cdot d \cdot (\beta_{max} - \beta_{min})$ is the coincidence time window with c being the speed of light, d the flight path from the target to the detector, and β_{min} and β_{max} corresponding to the lowest and highest momentum neutrons of interest (about 300 and 1000 MeV/c in our case). As $R_{e-singles}$ and $R_{n-singles}$ each scale linearly with luminosity, R_{BG} scales quadratically, This makes the signal-to-background ratio scale linearly with luminosity, i.e. x10 higher as compared to CLAS6 running conditions. In the case of reactions involving leading high-momentum (> 1 GeV/c) neutrons such as $(e, e'n)$ and $(e, e'np)$ in QE kinematics this increase will not have a significant impact as the background level in CLAS6 was observed to be approximately 1% or less [32].

The more challenging situation is the detection of low-momentum recoil neutrons. We start by concidering the BG levels in CLAS6 as observed in our ongoing analysis of A$(e, e'pn)$ reactions off C and Fe targets with a 5 GeV/c incident beam in SRC kinematics that are equivalent to the current proposal. For recoil neutrons detected in the CLAS6 TOF scintillators, we observe a signal-to-background ratio of 1:3 (see Fig. 24). While previous Hall-A analyses successfully handled signal to background ratios up to about 1:10 with only several hundred signal events, a ratio

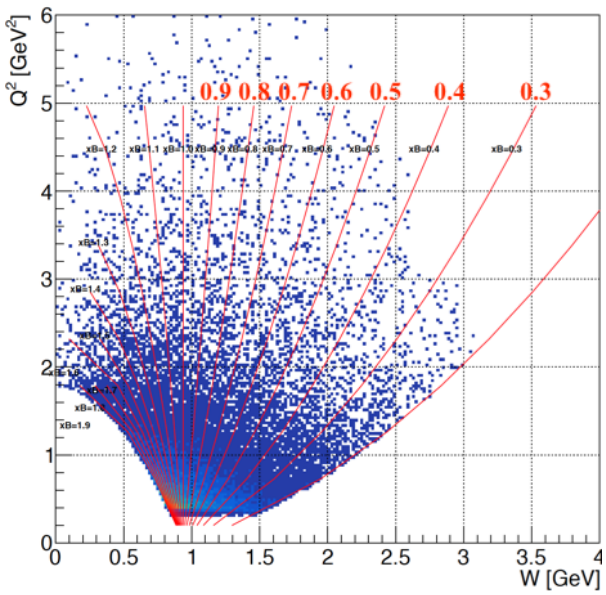

FIG. 23: Momentum transfer Q^2 versus W for a 6.6 GeV incident beam, where only events with x_B between 0.2 and 1.9 are considered. The red lines are labeled for constant x_B. The hard DIS regime ($W > 1.8$ GeV and $Q^2 > 1.5$ GeV^2) covers up to $x \sim 0.7$, which will cover the full regime relevant to EMC studies.

of 1:30 would be challenging, even with an increased signal statistics. However, in the case of the central neutron detector, the reduced neutron flight-path, as compared to that of the CLAS6 TOF counters, reduces the coincidence time window of recoil neutron events of interest with reduces the random coincidence rate. This reduction in the coincidence time window compensates for the increased luminosity, leading to a manageable 1:3–1:5 Signal:BG ratio in recoil neutron detection channels.

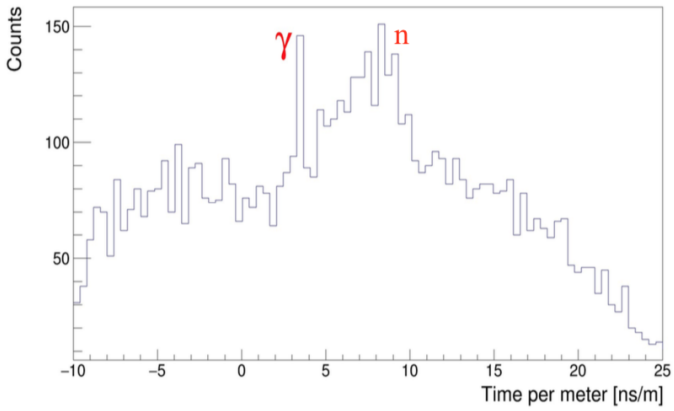

FIG. 24: The measured CLAS6 neutral hit time spectra for Fe$(e, e'pn)$ events in SRC kinematics. The neutral hits are detected in the CLAS6 TOF scintillators over a wide kinematical regime. A clear gamma peak at 3.3 ns/m is seen, followed by a neutron peak with a signal-to-background ratio of about 1:3.

While we are interested in using 4.4 and 6.6 GeV beams, we are not sensitive to the precise beam energies used and can accommodate changes to the exact energy as required by the accelerator and experimental scheduling. The 6.6 GeV beam energy optimizes the combination of cross-section (i.e., rate) and missing momentum resolution. The 4.4 GeV beam energy will provide a cross-check to the data at 6.6 GeV with an improved missing momentum resolution, leading neutron detection and will be used to study the Q^2 dependence.

B. Rate Estimation and beam time request

The rate estimation is done by scaling the measured $A(e,e'Np)$ events rates from the CLAS6 EG2 experiment [6]. The experiment ran for 25 PAC days at an incident beam energy of 5 GeV on solid targets (C, Al, Fe, Pb, and Sn) held simultaneously with a deuterium target cell in the beam. The primary considerations that go into the scaling from CLAS6 include a factor of 10 increase in luminosity (from 10^{34} to 10^{35} cm^{-2}s^{-1}) and a conservative factor of 2 increase to account for the solid angle acceptance, Mott cross-section (fot 6.6 GeV) and recoil detection. The number of $A(e,e'Np)$ events measured in EG2 is given in Table I above, while Table II below details the number of beam days used for each target. In EG2, the thickness of the solid and deuterium targets was chosen such that the luminosity was divided equally between the two (with the exception of lead which is half as thick). As we do not wish to measure deuterium in parallel to the solid targets, we scale the rate to 100% luminosity on the solid target.

TABLE II: Number of PAC days per target in the CLAS6 EG2 experiment, adjusting for 100% luminosity on the solid target.

Target	**Beam days**
C+D	2.5
Al	1.25
Fe+D	5.5
Pb+D	11.5
Sn+D	0.25
Total: 21	

Unlike EG2, we wish to obtain comparable statistics for all targets at 6.6 GeV, with the exception of ^{4}He where we wish to get more statistics than the other targets and ^{208}Pb where we expect to obtain half the statistics due to the luminosity reduction by a factor of two. We extrapolated from the measured EG2 rate for ^{12}C and then calculated all other nuclei assuming that the outgoing nucleon attenuation scales as $A^{1/3}$. Deuterium will also require more beam-time as it has a smaller fraction (factor of $\sim$4) of its momentum density at high-momentum. The statistics that we wish to obtain at 4.4 GeV will supplement the measurements taken at the higher beam energy and allow for energy-dependent studies. The statistics of each target at 4.4 GeV are not uniformly chosen as in the statistics at 6.6 GeV.

We request a total of 39 PAC days (to include the pass change) of which 30 PAC days are at 6.6 GeV and 8 PAC days are at 4.4 GeV. At 6.6 GeV, this includes 27 days of beam on target, 1 day for calibration, and 2 days for target changes. The two days for target changes are to install and remove the Ca target capsule and for any changes needed to switch from D to ^{4}He. At 4.4 GeV, the 1 day for target change is for the switch from D to ^{4}He. The requested beam-time for each target is shown in Table III.

TABLE III: Requested beam time per target, including calibration time and target change overhead.

Target:	**d**	**^{4}He**	**^{12}C**	**^{28}Si**	**^{40}Ca**	**^{48}Ca**	**^{120}Sn**	**^{208}Pb**	**Total**
Measurement Days (6.6 GeV)	5	3	2	2	3	3	4	5	**27**
Calibration									**1**
Target Changes									**2**
								Total at 6.6 GeV:	**30**
Measurement Days (4.4 GeV)	2	1	1	0	0	0	1	1	**6**
Calibration									**1**
Target Changes									**1**
								Total at 4.4 GeV:	**8**

The expected number of events for the two and three nucleon knockout reactions in ^{12}C are listed in Table IV. The rates for the other solid targets will be equivalent, except for Pb which will be cut by a factor of 2 due to the maximal luminosity that can be applied to this target. ^{4}He will have a factor of 2 higher statistics. The single nucleon knockout and inclusive reactions event rates are typically larger by one to two orders of magnitude.

VI. RELATION TO OTHER APPROVED 12 GEV MEASUREMENTS

Due to the large acceptance and open trigger of the CLAS12, the obtained data set will include electron scattering reactions with anything between zero and three nucleons in the final state. In the context of SRCs, **there are no**

TABLE IV: Expected number of counts for various 2N and 3N knockout reactions for each target/beam energy. The reaction notation is that the first nucleon is the "leading" nucleon (i.e., a high-momentum nucleon that is emitted largely in the momentum transfer direction) and all other nucleons are the recoil nucleons.

	2N-SRC				3N-SRC		
Reaction	$(e,e'pp)$	$(e,e'pn)$	$(e,e'np)$	$(e,e'nn)$	$(e,e'ppp)$	$(e,e'pnp)$	$(e,e'npp)$
# events (6.6 GeV)	13k	13k	8.5k	250	2k	200	200
# events (^{208}Pb at 6.6 GeV)	6.5k	6.5k	4.3k	125	1k	100	100
# events (^{12}C at 4.4 GeV)	3.4k	3.4k	2.2k	64	0.5k	52	52
# events (^{120}Sn and ^{208}Pb each at 4.4 GeV)	1.3k	1.3k	0.9k	25	0.2k	20	20
# events (^{4}He at 4.4 GeV)	4.8k	4.8k	3.2k	93	0.7k	74	74

12 GeV experiments approved to measure exclusive reactions with two and three nucleons in the final state, which is the primary focus of the current proposal.

Several of the spokespersons of the current proposal are also co-spokespersons of E12-14-011 [53] and E12-17-005 [63] that will study the semi-inclusive $A(e,e'p)$ reaction in ^{3}He, ^{3}H, ^{40}Ca and ^{48}Ca, in kinematics sensitive to SRCs. The current proposal does not overlap with the ^{3}He and ^{3}H measurements. It might appear to have some overlap with the Ca isotopes measurement, however that proposal will extract detailed absolute cross-sections as a function of missing momentum and energy that can only be studied using high-luminosity, high-resolution spectrometers and cannot be done using CLAS12. Simillarly, due to the inclusive nature of the CLAS12 trigger we will collect some (e,e') data. This is not the focuse of this proposal and will include primerally data on nuclei that were previously studied as part of the 6 GeV program and in kinematics that are not comperable to the 12 GeV spectrometers expriments.

A. Run group proposal with Electrons for Neutrinos

This proposed experiment can run along with the Electron for Neutrinos proposal as run group, using the CLAS12 detector in its standard configuration. By running these experiments together, targets, beam time, and calibrations can be shared in addition to the complementary nature of the physics to be studied. These experiments will take data at common beam energies of 4.4 and 6.6 GeV on several of the same targets. They will overlap on a total of 9 days at 4.4 and 6.6 GeV. The information obtained in both experiments is useful for understanding detector-related efficiencies and reconstruction effects, as well as contributions from FSIs and other reaction mechanisms that are important for of both analyses. The Short-Range Correlations in Nuclei proposal will expand the nuclear mass range over a wide phase space in kinematical coverage which will directly improve the data we take in the Electron for Neutrinos proposal.

[1] O. Hen, G. A. Miller, E. Piasetzky, and L. B. Weinstein, Rev. Mod. Phys. **89**, 045002 (2017), 1611.09748.
[2] C. Ciofi degli Atti, Phys. Rept. **590**, 1 (2015).
[3] J. Carlson, S. Gandolfi, F. Pederiva, S. C. Pieper, R. Schiavilla, K. E. Schmidt, and R. B. Wiringa, Rev. Mod. Phys. **87**, 1067 (2015), 1412.3081.
[4] J. Arrington, D. W. Higinbotham, G. Rosner, and M. Sargsian, Prog. Part. Nucl. Phys. **67**, 898 (2012), 1104.1196.
[5] L. Frankfurt, M. Sargsian, and M. Strikman, Int. J. Mod. Phys. **A23**, 2991 (2008), 0806.4412.
[6] O. Hen et al., Science **346**, 614 (2014), 1412.0138.
[7] I. Korover et al. (Lab Hall A), Phys. Rev. Lett. **113**, 022501 (2014), 1401.6138.
[8] R. Subedi et al., Science **320**, 1476 (2008), 0908.1514.
[9] E. Piasetzky, M. Sargsian, L. Frankfurt, M. Strikman, and J. W. Watson, Phys. Rev. Lett. **97**, 162504 (2006), nucl-th/0604012.
[10] N. Fomin et al., Phys. Rev. Lett. **108**, 092502 (2012), 1107.3583.
[11] K. S. Egiyan et al. (CLAS), Phys. Rev. Lett. **96**, 082501 (2006), nucl-ex/0508026.
[12] L. L. Frankfurt, M. I. Strikman, D. B. Day, and M. Sargsian, Phys. Rev. **C48**, 2451 (1993).
[13] L. B. Weinstein, E. Piasetzky, D. W. Higinbotham, J. Gomez, O. Hen, and R. Shneor, Phys. Rev. Lett. **106**, 052301 (2011), 1009.5666.
[14] O. Hen, E. Piasetzky, and L. B. Weinstein, Phys. Rev. **C85**, 047301 (2012), 1202.3452.
[15] O. HEN, D. W. HIGINBOTHAM, G. A. MILLER, E. PIASETZKY, and L. B. WEINSTEIN, International Journal of Modern Physics E **22**, 1330017 (2013), https://www.worldscientific.com/doi/pdf/10.1142/S0218301313300178, URL https://www.worldscientific.com/doi/abs/10.1142/S0218301313300178.
[16] D. Higinbotham, G. A. Miller, O. Hen, and K. Rith, CERN Cour. **53N4**, 24 (2013), 1305.7143.
[17] O. Hen, A. Accardi, W. Melnitchouk, and E. Piasetzky, Phys. Rev. **D84**, 117501 (2011), 1110.2419.
[18] O. Hen, B.-A. Li, W.-J. Guo, L. B. Weinstein, and E. Piasetzky, Phys. Rev. **C91**, 025803 (2015), 1408.0772.
[19] B.-A. Li, B.-J. Cai, L.-W. Chen, and J. Xu, Prog. Part. Nucl. Phys. **99**, 29 (2018), 1801.01213.
[20] B.-A. Li, W.-J. Guo, and Z. Shi, Phys. Rev. **C91**, 044601 (2015), 1408.6415.
[21] G. A. Miller, A. Beck, S. May-Tal Beck, L. B. Weinstein, E. Piasetzky, and O. Hen (2018), 1805.12099.
[22] O. Hen, L. B. Weinstein, E. Piasetzky, G. A. Miller, M. M. Sargsian, and Y. Sagi, Phys. Rev. **C92**, 045205 (2015), 1407.8175.
[23] M. M. Sargsian, Phys. Rev. **C89**, 034305 (2014), 1210.3280.
[24] M. Martini, M. Ericson, and G. Chanfray, Phys. Rev. **D85**, 093012 (2012), 1202.4745.
[25] H. Gallagher, G. Garvey, and G. P. Zeller, Ann. Rev. Nucl. Part. Sci. **61**, 355 (2011).
[26] R. Weiss, R. Cruz-Torres, N. Barnea, E. Piasetzky, and O. Hen, Phys. Lett. **B780**, 211 (2018), 1612.00923.
[27] R. Cruz-Torres, A. Schmidt, G. A. Miller, L. B. Weinstein, N. Barnea, R. Weiss, E. Piasetzky, and O. Hen (2017), 1710.07966.
[28] F. Simkovic, A. Faessler, H. Muther, V. Rodin, and M. Stauf, Phys. Rev. **C79**, 055501 (2009), 0902.0331.
[29] D. Lonardoni, S. Gandolfi, X. B. Wang, and J. Carlson (2018), 1804.08027.
[30] S. N. More, S. K. Bogner, and R. J. Furnstahl, Phys. Rev. **C96**, 054004 (2017), 1708.03315.
[31] O. Hen et al. (CLAS), Phys. Lett. **B722**, 63 (2013), 1212.5343.
[32] M. Duer et al. (CLAS), Submitted (2017).
[33] A. Tang et al., Phys. Rev. Lett. **90**, 042301 (2003), nucl-ex/0206003.
[34] R. Shneor et al. (Jefferson Lab Hall A), Phys. Rev. Lett. **99**, 072501 (2007), nucl-ex/0703023.
[35] M. Duer et al. (CLAS), under internal review (2018).
[36] R. Schiavilla, R. B. Wiringa, S. C. Pieper, and J. Carlson, Phys. Rev. Lett. **98**, 132501 (2007), nucl-th/0611037.
[37] M. M. Sargsian, T. V. Abrahamyan, M. I. Strikman, and L. L. Frankfurt, Phys. Rev. **C71**, 044615 (2005), nucl-th/0501018.
[38] M. Alvioli, C. Ciofi degli Atti, and H. Morita, Phys. Rev. Lett. **100**, 162503 (2008).
[39] R. B. Wiringa, R. Schiavilla, S. C. Pieper, and J. Carlson, Phys. Rev. C **89**, 024305 (2014), URL https://link.aps.org/doi/10.1103/PhysRevC.89.024305.
[40] C. Colle, O. Hen, W. Cosyn, I. Korover, E. Piasetzky, J. Ryckebusch, and L. B. Weinstein, Phys. Rev. **C92**, 024604 (2015), 1503.06050.
[41] C. Colle, W. Cosyn, and J. Ryckebusch, Phys. Rev. **C93**, 034608 (2016), 1512.07841.
[42] W. U. Boeglin et al. (Hall A), Phys. Rev. Lett. **107**, 262501 (2011), 1106.0275.
[43] L. L. Frankfurt, M. M. Sargsian, and M. I. Strikman, Phys. Rev. **C56**, 1124 (1997), nucl-th/9603018.
[44] C. Colle, W. Cosyn, J. Ryckebusch, and M. Vanhalst, Phys. Rev. **C89**, 024603 (2014), 1311.1980.
[45] D. Dutta, K. Hafidi, and M. Strikman, Prog. Part. Nucl. Phys. **69**, 1 (2013), 1211.2826.
[46] L. Frankfurt, M. Strikman, and M. Zhalov, Phys. Lett. **B503**, 73 (2001), hep-ph/0011088.
[47] V. R. Pandharipande and S. C. Pieper, Phys. Rev. **C45**, 791 (1992).
[48] M. Alvioli, C. Ciofi degli Atti, and H. Morita, Phys. Rev. **C94**, 044309 (2016), 1607.04103.
[49] M. Alvioli, C. Ciofi degli Atti, L. P. Kaptari, C. B. Mezzetti, H. Morita, and S. Scopetta, Phys. Rev. **C85**, 021001 (2012), 1112.2651.
[50] S. Fucini, S. Scopetta, and M. Viviani (2018), 1805.05877.
[51] E. O. Cohen, O. Hen, E. Piasetzky, L. B. Weinstein, M. Duer, A. Schmidt, I. Korover, and H. Hakobyan (CLAS) (2018),

1805.01981.
[52] C. Ciofi degli Atti and S. Simula, Phys. Rev. **C53**, 1689 (1996), nucl-th/9507024.
[53] O. Hen et al., JLab Experiment E12-14-011 (2014).
[54] O. Hen, L. B. Weinstein, S. Gilad, and W. Boeglin (2014), 1410.4451.
[55] B. Schmookler et al. (CLAS), Submitted (2018).
[56] D. W. Higinbotham and O. Hen, Phys. Rev. Lett. **114**, 169201 (2015), 1409.3069.
[57] Z. Ye et al. (Hall A) (2017), 1712.07009.
[58] N. Fomin, D. Higinbotham, M. Sargsian, and P. Solvignon, Ann. Rev. Nucl. Part. Sci. **67**, 129 (2017), 1708.08581.
[59] D. B. Day, L. L. Frankfurt, M. M. Sargsian, and M. I. Strikman (2018), 1803.07629.
[60] J. Kelly, Adv. Nucl. Phys. **23**, 75 (1996).
[61] M. Sargsian, *Private communication*.
[62] F. Benmokhtar et al. (Jefferson Lab Hall A Collaboration), Phys. Rev. Lett. **94**, 082305 (2005).
[63] . Hen, O et al., JLab Experiment E12-17-004 (2017).